JOURNAL OF PETROLOGY | VOLUME 41 | NUMBER 8 | PAGES 1329–1364 | 2000

H_2O Abundance in Depleted to Moderately Enriched Mid-ocean Ridge Magmas; Part I: Incompatible Behaviour, Implications for Mantle Storage, and Origin of Regional Variations

LEONID V. DANYUSHEVSKY[1]*, STEPHEN M. EGGINS[2], TREVOR J. FALLOON[1] AND DAVID M. CHRISTIE[3]

[1]SCHOOL OF EARTH SCIENCES, UNIVERSITY OF TASMANIA, GPO BOX 252-79, HOBART, TAS. 7001, AUSTRALIA

[2]ARC KEY CENTRE FOR GEOCHEMICAL EVOLUTION AND METALLOGENY OF THE CONTINENTS (GEMOC), DEPARTMENT OF GEOLOGY; AND RESEARCH SCHOOL OF EARTH SCIENCES; AUSTRALIAN NATIONAL UNIVERSITY, GPO BOX 4, CANBERRA, A.C.T. 2601, AUSTRALIA

[3]COLLEGE OF OCEANIC AND ATMOSPHERIC SCIENCES, 104 OCEAN ADMINISTRATION BUILDING, OREGON STATE UNIVERSITY, CORVALLIS, OR 97331-5503, USA

RECEIVED AUGUST 25, 1999; REVISED TYPESCRIPT ACCEPTED JANUARY 14, 2000

The H_2O contents and trace-element abundances are presented for two well-studied suites of mid-ocean ridge basalt (MORB) glasses from the Northern East Pacific Rise (EPR, 9–11°N) and the South East Indian Ridge (SEIR, 127–129°E). Exactly the same region of the glass samples has been analysed for these components using microbeam techniques. Our data allow examination of the fine details of H_2O geochemical behaviour during MORB genesis. We demonstrate that relative H_2O contents [i.e. H_2O/(another incompatible element)] vary systematically with increasing $(La/Sm)_N$ in MORB glasses from both the EPR and SEIR. This indicates that H_2O behaves like other incompatible (in peridotite mineralogies) elements during MORB petrogenesis, and is primarily controlled by solid–melt partitioning. However, the relative H_2O contents of MORB glasses from the SEIR are higher than in glasses from the EPR at a given $(La/Sm)_N$, demonstrating global variations in the H_2O contents of MORB. Despite regional differences in relative H_2O contents, the incompatible behaviour of H_2O is similar in both studied regions. The relative incompatibility of H_2O varies systematically with increasing $(La/Sm)_N$: in depleted MORB, H_2O is similar to La whereas in EMORB, H_2O is similar to Ce. Similar patterns of varying relative incompatibility (to REE) are displayed by Zr, Hf, and P. Our data are best explained if H_2O is stored in the mantle in the same phase with LREE (clinopyroxene?) at sub-solidus. Regional variations in relative H_2O contents in EMORB that have more radiogenic Sr, Nd and Pb isotopes might be explained by differences in the nature of enriched components recycled via subduction processes. However, when EMORB have the same radiogenic isotope compositions as NMORB within a segment, relative H_2O contents in EMORB probably reflect local processes that lead to enrichment in incompatible elements. Regional differences in relative H_2O contents of NMORB may reflect either initial variations in the Earth's mantle or inhomogeneities left after formation of the continental crust.

KEY WORDS: *glass; geochemistry; H_2O; MORB; petrology*

INTRODUCTION

The H_2O contents of mid-ocean ridge basalts (MORB) has received much attention in the literature (Michael &

*Corresponding author. Telephone: +61-3-62262469. Fax: +61-3-62232547. e-mail: L.Dan@utas.edu.au

Chase, 1987; Aggrey *et al.*, 1988; Jambon & Zimmermann, 1990; Michael, 1995, 1988; Sobolev & Chaussidon, 1996; and references therein). Although it is a minor component in MORB, H_2O can significantly affect mantle melting and melt crystallization processes. For example, H_2O significantly decreases the solidus temperature (T) of peridotite (e.g. Green, 1976), and H_2O in basalt magma both depresses the liquidus temperature and delays crystallization of plagioclase (e.g. Sinton & Fryer, 1987). Mantle rheology and magma viscosity are also a function of H_2O content (e.g. Hirth & Kohlstedt, 1996). Thus, an understanding of the H_2O geochemistry of MORB is important for models of mantle composition, melting T, evolution and metasomatism, and crust recycling processes. The study of H_2O in MORB is facilitated by the fact that most MORB glasses are undersaturated in H_2O at the depths of eruption (e.g. Byers *et al.*, 1983; Dixon *et al.*, 1995) and retain their original H_2O content (see further discussion below). This assumption has been supported by comparison of H_2O contents in erupted glasses with those in melt inclusions in MORB phenocrysts trapped at greater depth in magma chambers before eruption (Sobolev & Chaussidon, 1996).

It is generally accepted that H_2O contents in the MORB mantle source range from 100 to 450 ppm (e.g. Michael, 1988; Sobolev & Chaussidon, 1996), accommodated by nominally anhydrous mantle minerals [i.e. olivine, pyroxenes, and garnet; Bai & Kohlstedt (1992); Bell & Rossman (1992); Hirth & Kohlstedt (1996)]. Michael (1995) attributed regional H_2O variations in the MORB mantle source ultimately to the recycling processes at subduction zones. In contrast, Bell (1996) argued that H_2O in the MORB source can, in general, be sustained by input from relatively undegassed deep mantle, and does not require additional H_2O contribution from subduction. Arguments for the efficient return of subducted H_2O back into the exosphere by supra-subduction zone processes (and thus minimum contribution of subduction to the H_2O balance of the MORB mantle source) are based on H_2O contents of relatively undegassed supra-subduction zone melts trapped as melt inclusions in high-Mg olivine (Sobolev & Chaussidon, 1996), and on relative [compared with rare earth elements (REE)] H_2O incompatibility in backarc basin basalts and MORB (Bell, 1996). However, it is important to bear in mind that the global H_2O cycle, especially the fluxes among mantle and crustal reservoirs, and the ability of subducting slabs to carry H_2O down into the mantle, is at present not well constrained (e.g. Schmidt & Poli, 1998).

The relationship between H_2O and other incompatible elements during melting of the MORB mantle source is controversial. Michael (1988, 1995) suggested that the similarity of H_2O/Ce values in normal (NMORB) and enriched (EMORB) MORB within a given region implies similar incompatibility of H_2O and Ce during evolution of the MORB mantle source. If so, different H_2O/Ce values in MORB glasses from different regions should indicate variations in source compositions. On the basis of a compilation of H_2O and trace-element data, Michael (1995) demonstrated that H_2O/Ce values are similar in MORB from the American–Antarctic Ridge, Southwest Indian Ridge, southern Mid-Atlantic Ridge (MAR), Pacific Nazca Ridge, East Pacific Rise (EPR) around 10–12°N, Galapagos spreading centre, Explorer Ridge, and Mid-Cayman Rise spreading centre, averaging about 150–220. In contrast, northern MAR glasses are characterized by significantly higher H_2O/Ce values (240–280). These data were interpreted by Michael (1995) to result from a higher contribution of subducted altered oceanic crust to the mantle source of MORB under the North Atlantic.

Dixon *et al.* (1988) suggested that H_2O has similar incompatibility to La in samples from the Juan de Fuca Ridge. Jambon & Zimmermann (1990) argued that the constant K_2O/H_2O ($\sim$0·25) of NMORB is inherited unmodified by partial melting variations, and reflects the K_2O/H_2O of the mantle sources. According to Jambon & Zimmermann (1990), all MORB with higher K_2O/H_2O values are produced from a metasomatized mantle source [e.g. produced by mixing of an NMORB mantle source with some other metasomatizing (or mixing) agent with $K_2O/H_2O \sim 1{\cdot}5$, probably derived from recycled crust]. In general, the idea that the mantle source of MORB represents a mixture of two or more components is supported by many studies (e.g. Zindler *et al.*, 1984; Niu *et al.*, 1996; Niu & Batiza, 1997).

In this paper, we present data on H_2O contents for $\sim$100 MORB glasses from Lamont Seamounts, ridge-crest and off-axis locations at 9–11°N, EPR, and from the ridge crest at 127–129°E, South East Indian Ridge (SEIR). The glass compositions span the MORB spectrum from highly depleted NMORB [$(La/Sm)_N \sim 0{\cdot}3$, where N indicates primitive-mantle normalized] to moderately enriched EMORB compositions [$(La/Sm)_N \sim 1{\cdot}4$]. In both suites, the relative incompatibility of H_2O (i.e. incompatibility compared with REE) is identical and varies systematically with increasing $(La/Sm)_N$. In samples with $(La/Sm)_N < \sim 0{\cdot}85$, H_2O behaves similarly to La whereas in more enriched samples H_2O is similar to Ce. H_2O is more compatible than K_2O at all values of $(La/Sm)_N$. Our data also demonstrate that the relative H_2O contents of MORB glasses from the SEIR and EPR are distinct at a given $(La/Sm)_N$, confirming the presence of significant regional variations (Michael, 1995).

ANALYTICAL TECHNIQUES

Most of our data [H_2O by Fourier Transform infrared (FTIR) spectroscopy, major elements by electron

microprobe, and trace elements by laser ablation inductively coupled plasma mass spectroscopy (LA-ICP-MS)] were obtained on the same area (within 2–3 mm) of a single glass chip. For ridge-crest and normal-crust off-axis glasses from locations at 9–11°N EPR, trace elements were analysed by instrumental neutron activation analysis (INAA) (Batiza & Niu, 1992; R. Batiza, unpublished data, 1996) on different splits of the same glass samples.

FTIR spectroscopy

The H_2O concentrations in glasses were determined using a Bruker IFS 66 spectrometer with attached optical microscope with all-reflecting optics and Bruker Opus/IR reduction software; the calibration and procedures of Danyushevsky *et al.* (1993) were followed (H_2O contents were analysed using the main OH-stretching peak at $\sim$3500 cm^{-1}; during each analysis, 100 scans were collected with a resolution of four wavenumbers between 4000 cm^{-1} and 2400 cm^{-1}). Doubly polished sections of glass (50–250 μm thick, 2–5 mm in diameter) (one for each glass sample) were analysed 2–6 times (Table 1). The diameter of the analysed areas was usually 60 μm to ensure that no microlites were present in the analysed volume. The range of H_2O contents for each glass is reported in Table 1. Most our glasses show no H_2O variations between individual analyses in a single glass chip exceeding the reproducibility of repetitive analyses on the same spot (2–3%). However, variations slightly larger than this (up to 8%), were found in two glasses from the EPR axis at 9·5°N (R44-6 and R59-1, Table 1). No systematic pattern of H_2O variations was observed in these anomalously heterogeneous glasses, and we used average H_2O contents to characterize them. The accuracy of the calibration of Danyushevsky *et al.* (1993) for MORB glasses can be addressed by comparing analyses of the same samples carried out in different laboratories and is estimated to be within 5% relative (L. V. Danyushevsky & P. J. Michael, unpublished data, 1996).

We also note that in glasses from the EPR axis at 9·5°N, alteration around numerous light-coloured glassy veins that are 10–20 μm thick (and extending up to 200–300 μm away from these veins) results in increased H_2O contents in visually unaltered glass. However, K_2O and other major elements around such veins appear to be unaltered. For these glasses we report H_2O contents measured at a sufficient distance away from the veins to avoid this problem.

Electron microprobe

Compositions of glasses were analysed using a Cameca SX50 electron microprobe at the University of Tasmania, Hobart, at 15 kV and 20 nA, using international standard USNM 111240/2 (basaltic glass) from Jarosewich *et al.* (1980). Counting times for all elements except K were 10 s for the peak and 5 s for the background on both sides of the peak. K was analysed for 30 s on the peak and 15 s on the background. In glasses with very low K contents (<0·04 wt %) analyses were performed with 60 s counting times for the peak and background on both sides. We routinely used a beam size of $\sim$5 μm, except for glasses with very low K contents, for which we used $\sim$20 μm. No variations in major elements exceeding standard electron microprobe accuracy (2% for Si, Al, Fe, Mg, and Ca; 5% for Na and Ti; 5–50% for K depending on the absolute content from 0·8 to 0·010 wt %) were found. Chlorine analyses in the Lamont Seamount glasses were performed with 100 s counting time for the peak and background on both sides using a beam size of 10 μm and current of 50 nA.

LA-ICP-MS

Trace elements were measured by LA-ICP-MS at the Research School of Earth Sciences, Australian National University. The instrumentation employs a pulsed ArF (193 nm) EXCIMER laser that is coupled to a Fisons PQ2 STE quadruple ICP-MS instrument, via a custom-built beam delivery and ablation cell system. A more detailed description of the system and its performance characteristics has been given by Eggins *et al.* (1998*a*, 1998*b*). For this study, analysis was performed by ablating circular spots of 125 and 200 μm diameter, using a power density of $\sim$0·5 GW and a laser pulse rate of five repetitions per second, in a He atmosphere. The resultant etch rate is $\sim$0·5 μm/s and >90% transport efficiency to the ICP instrument is achieved for the ablated material. The instrument was optimized for sensitivity on mid- to high-mass isotopes (in the range 80–240 a.m.u.) and for minimal molecular oxide species production (i.e. $^{232}Th^{16}O/^{232}Th$ <0·4%) by ablating an NIST612 glass. Instrument sensitivity varies as a function of mass, isotopic abundance, ionization efficiency of the element in the ICP, and the mass ablation rate, and for most analysed isotopes reported herein is in the range 1000–10 000 c.p.s./ppm. The low level of molecular oxide production precludes the need to correct any of the analyte signal intensities for interfering species. Each analysis involves sequential peak hopping through the mass spectrum, with the accumulation of 80 replicate measurements of $\sim$30 ms duration (2·4 s total) for each of the 25 or so analyte isotopes. The analysis time for each sample was 140 s, comprising a 60 s background and 80 s analysis with laser-on for a total of 2 s duty cycle on each peak with laser-on. Instrument calibration was performed by ablating the NIST612 glass standard. Repeat analyses of

Table 1: H_2O, major element, and Cl concentrations in the studied glasses

Sample	Comments	Group	No. 1	No. 2	SiO_2	TiO_2	Al_2O_3	FeO*	MnO	MgO	CaO	Na_2O	K_2O	P_2O_5	Cr_2O_3	H_2O	Cl
Zero-age 9·3–9·7°N EPR																	
R37-1	1	—	4	4	50·78	1·59	14·52	10·89	0·16	7·35	11·72	2·62	0·11(2)	0·15	0·01	0·184(2)	—
R38-1	1	—	4	4	50·75	1·68	14·45	11·12	0·13	7·00	11·54	2·53	0·13(1)	0·17	0·03	0·207(5)	—
R39-1	1	—	3	6	51·37	1·56	14·99	10·72	0·14	7·60	12·02	2·39	0·14(1)	0·16	0·04	0·205(5)	—
R41-1	1	—	4	4	50·88	1·62	14·80	10·72	0·13	6·80	12·02	2·48	0·12(2)	0·17	0·04	0·209(3)	—
R44-6	1,7	—	5	4	50·84	1·60	14·54	10·74	0·11	7·28	11·85	2·47	0·13(1)	0·16	0·04	0·202(11)	—
R46-2	1	—	5	4	50·82	1·64	14·95	10·63	0·13	6·95	11·88	2·61	0·14(1)	0·17	0·03	0·202(4)	—
R47-3	1	—	3	4	50·65	1·34	15·16	9·76	0·16	7·89	12·20	2·40	0·13(1)	0·14	0·06	0·160(3)	—
R48-1	1	—	4	4	50·87	1·61	14·71	10·72	0·11	7·20	11·76	2·48	0·13(1)	0·19	0·03	0·198(4)	—
R50-1	1	—	4	4	50·42	1·23	15·67	9·34	0·13	8·49	12·26	2·34	0·103(1)	0·12	0·05	0·139(1)	—
R51-1	1	—	2	6	50·74	1·21	15·70	9·19	0·11	8·19	12·19	2·42	0·078(2)	0·12	0·05	0·125(1)	—
R52-1	1	—	4	4	50·78	1·59	14·93	10·55	0·14	7·32	11·83	2·51	0·11(1)	0·16	0·05	0·191(5)	—
R56-5	1	—	3	4	50·46	1·23	15·57	9·40	0·11	8·24	12·22	2·30	0·09(2)	0·15	0·07	0·149(4)	—
R59-1	1,7	—	5	4	50·58	1·66	14·55	10·81	0·19	7·22	11·58	2·53	0·13(0)	0·17	0·03	0·206(12)	—
Off-axis 9·5–11·3°N EPR																	
P2-3		9·5°N	4	6	50·37	2·33	14·29	11·79	0·21	5·80	10·65	3·15	0·44(1)	0·29	0·01	0·47(0)	—
P4-1		9·5°N	4	4	50·04	1·60	15·16	10·32	0·15	7·44	11·71	2·48	0·14(1)	0·13	0·04	0·20(1)	—
P22-1		9·5°N	4	4	50·83	1·64	14·86	10·41	0·15	6·81	11·66	2·80	0·32(1)	0·19	0·04	0·30(0)	—
P24-2		9·5°N	5	4	50·72	1·67	14·54	10·54	0·20	6·64	11·53	2·84	0·33(2)	0·18	0·05	0·31(1)	—
P59-2		10·5°N	4	4	50·66	2·36	13·57	12·69	0·21	6·04	10·67	2·75	0·22(2)	0·22	0·00	0·32(0)	—
P64-3		10·5°N	4	4	50·39	2·24	13·48	12·49	0·21	6·11	10·59	2·72	0·19(1)	0·22	0·02	0·30(0)	—
P65-1		10·5°N	4	4	50·37	2·49	13·07	13·61	0·20	5·50	10·01	2·90	0·20(1)	0·24	0·02	0·31(0)	—
P66-2		10·5°N	4	4	50·06	2·81	12·99	13·91	0·15	5·76	9·82	2·76	0·21(1)	0·25	0·03	0·31(1)	—
P100-1		11·3°N	4	4	50·69	2·05	14·08	11·54	0·22	6·23	11·19	2·85	0·24(1)	0·18	0·02	0·30(0)	—
P101-1		11·3°N	4	4	50·92	1·94	14·18	11·50	0·15	6·42	11·10	2·79	0·23(2)	0·21	0·03	0·29(0)	—
P102-1		11·3°N	5	4	50·40	1·78	14·90	10·39	0·21	6·86	11·67	2·77	0·20(1)	0·19	0·04	0·25(1)	—
P103-1		11·3°N	4	4	50·38	1·75	14·86	10·32	0·16	7·12	11·54	2·74	0·20(2)	0·16	0·04	0·24(0)	—
P104-1		11·3°N	4	4	50·41	1·73	14·76	10·43	0·17	6·94	11·45	2·69	0·25(2)	0·19	0·03	0·27(0)	—
P108-1		11·3°N	4	4	49·84	2·03	15·57	10·12	0·13	6·44	10·89	3·03	0·59(3)	0·28	0·04	0·44(0)	—
P109-1		11·3°N	5	4	49·65	1·54	15·97	9·42	0·16	7·49	11·89	2·80	0·21(0)	0·19	0·03	0·25(1)	—

Table 1: continued

Sample	Comments	Group	No. 1	No. 2	SiO_2	TiO_2	Al_2O_3	FeO*	MnO	MgO	CaO	Na_2O	K_2O	P_2O_5	Cr_2O_3	H_2O	Cl
Lamont Seamounts																	
F1-1	2	SASHA	2	4	50·66	1·16	15·34	9·14	0·15	8·22	12·82	2·25	0·081(3)	0·07	0·05	0·097(2)	15(5)
F2	2	SASHA	2	4	48·70	0·84	17·33	8·22	0·13	9·62	12·90	2·07	0·017(20)	0·06	0·09	0·054(0)	26(37)
F2-1	2	SASHA	4	4	48·59	0·82	17·41	8·29	0·14	9·68	12·84	2·08	0·021(5)	0·04	0·06	0·055(1)	17(12)
F3-4	2	SASHA	2	4	48·75	0·81	17·15	8·33	0·14	9·65	12·86	2·05	0·017(11)	0·01	0·04	0·042(1)	24(18)
1558-1657	2	SASHA	2	4	49·96	0·94	15·62	9·41	0·16	8·59	13·11	2·16	0·032(11)	0·05	0·09	0·060(0)	60(40)
1558-2014	2,3	SASHA	2	4	48·78	1·21	17·12	8·66	0·17	8·57	12·21	2·76	0·033(12)	0·11	0·08	0·122(2)	39(29)
1571-1936	2	NEW	5	4	49·53	1·36	15·78	9·63	0·15	7·92	12·27	2·74	0·064(10)	0·09	0·03	0·133(1)	151(32)
F9-1	2	MOK	5	4	48·81	1·14	16·62	8·64	0·17	9·19	12·20	2·44	0·089(9)	0·08	0·03	0·165(3)	33(20)
1564-1857	2	MOK	2	4	49·14	0·91	16·72	8·77	0·13	9·18	12·70	2·22	0·027(7)	0·05	0·05	0·058(0)	72(11)
1562-2112	2	MOK	2	4	50·13	1·26	15·12	9·88	0·16	7·77	12·63	2·57	0·045(4)	0·09	0·04	0·113(1)	115(40)
1570-1830	2	MOK	2	4	49·00	0·98	16·73	8·77	0·12	8·94	12·58	2·35	0·025(9)	0·03	0·09	0·063(1)	171(33)
1572-1727	2	DTD	2	4	49·19	1·08	16·78	8·82	0·13	8·58	12·41	2·59	0·051(11)	0·06	0·04	0·097(1)	82(39)
1572-1755	2	DTD	2	4	48·88	1·10	16·84	8·80	0·17	8·54	12·42	2·61	0·045(3)	0·11	0·04	0·095(1)	71(14)
1560-1651	2	MIB	2	4	49·90	1·06	15·83	9·31	0·14	7·71	12·78	2·42	0·046(6)	0·04	0·05	0·083(1)	275(39)
1560-1522/1	2,3,4	MIB	2	4	49·57	1·33	16·86	8·84	0·15	8·04	11·74	3·24	0·020(14)	0·14	0·07	0·172(1)	—
1560-1522/2	2,3,4	MIB	4	8	49·91	1·29	16·79	8·82	0·15	7·94	11·86	3·21	0·023(8)	0·13	0·04	0·168(1)	119(38)
1568-2014/1	2,4,5	MIB	2	4	50·08	1·14	15·13	9·80	0·14	7·21	12·89	2·48	0·036(15)	0·04	0·05	0·148(1)	135(18)
1568-2014/2	2,4,5	MIB	4	8	50·55	1·15	15·08	9·88	0·16	7·75	12·95	2·47	0·038(10)	0·08	0·05	0·140(3)	—
1569-1601	2	MIB	2	4	50·51	1·16	14·63	10·20	0·18	7·08	12·92	2·37	0·052(10)	0·03	0·07	0·083(1)	178(35)
127–129° E SEIR																	
1-1	6,8	1,A2	2	4	51·11	2·39	13·99	12·02	0·17	6·62	10·84	2·6	0·12(1)	0·23	0·03	0·35(1)	—
1-2	6,8	1,A2	2	4	50·82	2·48	13·74	12·44	0·21	6·42	10·65	2·74	0·11(1)	0·23	0·01	0·34(0)	—
10-10	6,8	1,A1	2	4	50·42	2·59	13·95	11·68	0·21	6·27	10·62	3·12	0·11(1)	0·28	0·05	0·41(1)	—
11-9	6,8	1,A2	2	4	50·64	1·9	14·54	10·72	0·18	7·16	11·21	2·88	0·06(1)	0·12	0·03	0·24(0)	—
13-20	6,8	1,A2	2	4	50·21	2·58	13·58	12·74	0·21	6·21	10·45	2·85	0·11(1)	0·26	0·01	0·36(1)	—
16-28	6,8	1,A2	2	4	50·62	1·46	15·49	9·14	0·17	7·63	12·12	2·96	0·06(1)	0·14	0·04	0·18(0)	—
16-9	6,8	1,A2	2	4	50·34	1·40	15·78	9·02	0·16	7·70	12·16	2·97	0·08(1)	0·11	0·04	0·18(0)	—
19-54	6,8	1,A1	2	4	50·61	2·52	14·10	11·72	0·13	6·58	10·75	2·91	0·13(1)	0·25	0·03	0·35(0)	—
3-2	6,8	1,A2	2	4	50·76	3·15	12·68	14·63	0·19	5·29	9·45	2·88	0·15(1)	0·29	0·03	0·46(2)	—
9-14	6,8	1,A1	2	4	50·52	1·95	14·67	10·30	0·18	7·20	11·41	3·00	0·08(1)	0·18	0·03	0·26(0)	—
9-17	6,8	1,A1	2	4	50·38	1·96	14·7	10·24	0·15	7·18	11·35	2·92	0·08(1)	0·19	0·04	0·28(0)	—
16-12	6,8	2,A2	2	4	50·06	1·64	16·77	8·73	0·14	7·79	11·24	3·07	0·19(1)	0·23	0·02	0·34(1)	—
16-2	6,8	2,A2	2	4	49·77	1·67	16·91	8·8	0·11	7·84	11·23	3·08	0·20(2)	0·2	0·03	0·35(0)	—
17-1	6,8	3,A1	2	4	50·72	1·29	15·83	8·93	0·17	8·40	11·82	2·72	0·04(1)	0·13	0·05	0·12(0)	—
17-18	6,8	3,A1	2	4	50·84	1·32	15·97	8·94	0·14	8·37	11·82	2·79	0·03(1)	0·13	0·06	0·13(0)	—

H_2O and major-element concentration in wt %, Cl in ppm; FeO*, all Fe as FeO; No. 1, number of H_2O analyses; No. 2, number of major-element analyses; numbers in parentheses for K_2O, H_2O, and Cl show maximum deviation from the average value in the last digit; totals for the electron microprobe analyses including H_2O are 99·0–100·7. Comments: 1, an example of the complete sample name: RAITT02-R37-1 for R37-1; 2, groups correspond to seamount names; 3, glasses with anomalously low K_2O contents; 4, two different glass chips were analysed from this sample; 5, glasses with anomalously high H_2O contents compared with the main trend; 6, an example of the complete sample name: MW8801-1-59 for 1-59; 7, glasses with variations in H_2O contents exceeding the accuracy of FTIR spectroscopy; 8, group numbers (1, 2, or 3) are followed by the ridge segment number (A1 or A2).

the NIST612 glass were used to bracket each block of 10–12 unknown samples, and a linear drift correction was applied to the analyte count rates for each unknown sample based on any variation in the repeat measurements of the NIST612 glass. Data reduction was performed according to standard methods (Longerich *et al.*, 1996), using ^{43}Ca as the internal standard isotope and CaO concentrations in the unknown glasses and NIST612 measured by electron microprobe. Data quality during each batch of samples has been monitored by analysis of two glass standards (USGS BCR2g and 864a—an in-house natural MORB glass standard). Long-term and within-run reproducibility of analyses for these glasses are typically better than 3% (1 SD), and accuracy is of the order of 5% or better based on available data for BCR2g.

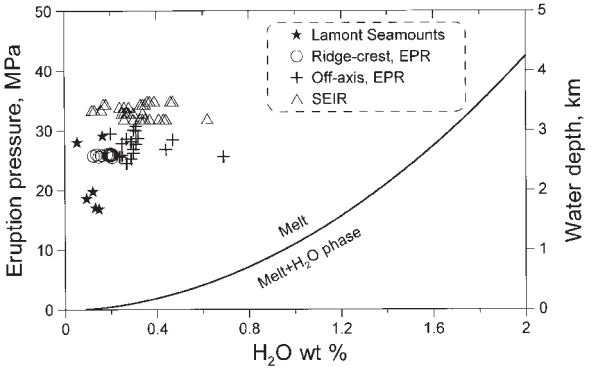

Fig. 1. Relationship between sampling water depths and glass H_2O contents. Continuous line represents the H_2O solubility curve for basaltic melts after Dixon *et al.* (1995). All glasses in this study are undersaturated in H_2O at the depths of eruption.

RATIONALE OF OUR DATA PRESENTATION

Our first aim is to establish the relative incompatibility of H_2O by examining variations of H_2O contents relative to La, Ce, and K_2O. Then we explore relationships among H_2O and major elements to evaluate possible controls of H_2O variations as a result of crystal fractionation and degree of partial melting. Covariations between H_2O and isotopic systematics are assessed for source heterogeneity effects. The cumulative result is that we identify many geochemically and petrologically distinct groupings of samples within each region.

Although approximately 100 glasses were analysed for H_2O and major-element contents, Table 1 presents only the data that also have trace-element abundances. However, in all figures involving only H_2O and major elements, the entire datasets are plotted. We emphasize that trace-element abundances have been analysed in representative samples of all geochemical groups identifiable by their H_2O and major-element compositions.

Magmatic origin of H_2O in analysed glasses

Two processes have the potential to alter the original melt H_2O contents in MORB glasses: degassing during eruption, which may lead to lower H_2O contents, and interaction with sea water, which may increase H_2O in glasses.

Dixon & Stolper (1995) demonstrated that the amount of H_2O that partitions into a CO_2-rich fluid phase in MORB magmas is critically dependent on the degree of H_2O undersaturation compared with a MORB magma at the same pressure (P) and T under pure-H_2O conditions. As it is well known that MORB magmas are CO_2 saturated and hence lose CO_2 during eruption, it is therefore possible for MORB magmas to lose H_2O as well, but this potential loss will depend on the degree of H_2O saturation. As can be seen in Fig. 1, measured H_2O contents of MORB glasses in this study are significantly undersaturated in H_2O compared with pure H_2O conditions. This means that H_2O loss during eruption must be insignificant and therefore will not be considered any further. This conclusion is supported by the fact that the maximum amount of vesicles in the studied glasses, even those with the highest H_2O contents, does not exceed 1 modal % (the maximum size of vesicles is <50 μm). For the Lamont Seamount glasses, a similar estimate was made by Allan *et al.* (1989).

To assess the possibility of sea-water contamination, we use correlations between glass H_2O contents and the contents of incompatible elements present in negligible amounts in sea water. If good correlations are present, there has presumably been negligible sea-water contamination, as widespread contamination should worsen or destroy these correlations. As will be shown below, most of the glasses from any one suite display strong positive correlations between H_2O and La or Ce, clearly supporting a magmatic origin for most of the analysed H_2O. Only one sample in our collection (from Lamont Seamounts) plots off such correlations towards higher H_2O content, and this sample is discussed in more detail.

EPR 9–11°N

A part of the ridge between 9 and 11°N is one of the best studied areas of the EPR (e.g. Batiza & Vanko, 1984; Langmuir *et al.*, 1986; Harpp *et al.*, 1991; Batiza & Niu, 1992; Perfit *et al.*, 1994). MORB glasses analysed in this study were collected from the EPR ridge crest between 9·3 and 9·7°N (Batiza & Niu, 1992), from normal crust (produced at the EPR spreading ridge) at off-axis locations at ~9·5°, 10·5°, and 11·3°N (Batiza *et al.*, 1996;

Niu *et al.*, 1999; Regelous *et al.*, 1999), and from the Lamont Seamounts (Fornari *et al.*, 1988; Allan *et al.*, 1989). Our data are compared with previously published H_2O contents of the northern EPR lavas in Appendix A.

Lamont Seamounts

The Lamont Seamount chain consists of five seamounts extending ~50 km westward from the EPR at ~10°N. Detailed petrological–geochemical studies of lavas recovered from these seamounts (Fornari *et al.*, 1988; Allan *et al.*, 1989) have shown that all glasses are relatively primitive (MgO between 7 and 9·5 wt %) and strongly depleted in incompatible elements, with $(La/Sm)_N$ ranging from 0·3 to 0·65. The combined trends of major-element variations resemble melt evolutionary paths along olivine + plagioclase ± clinopyroxene low-*P* cotectics (Allan *et al.*, 1989; Niu & Batiza, 1991). However, these same studies have shown that variations in incompatible-element contents cannot be accounted for by low-*P* fractionation processes alone, and imply that differences in the degree of melting and variable source compositions are involved.

H_2O geochemistry

Compositions of glasses analysed in this study are presented in Table 1. H_2O contents in the studied Lamont glasses vary in the range ~0·04–0·17 wt %. If this range was produced as a result of crystallization, we should expect a negative correlation between H_2O (an incompatible element) and MgO (a strongly compatible element). However, as clearly seen in Fig. 2a, there is a significant scatter in the MgO–H_2O plot. At the same time, a good positive correlation exists between H_2O and La and Ce contents for all but one sample (1568-2014, Fig. 2b and c). This correlation implies that, in general, variations in H_2O contents are not random, but controlled by the same factors that control the abundances of incompatible elements in MORB systems.

Anomalous sample 1568-2014 has significantly higher H_2O for a given La or Ce content compared with other samples. A duplicate analysis of another glass chip from this sample confirms its anomalous characteristics (Fig. 2, Tables 1 and 2). To evaluate the possibility of seawater contamination of this sample, we have analysed Cl contents in Lamont Seamount glasses (Table 1). Sample 1568-2014 does not have anomalous Cl contents, suggesting the high H_2O content in this sample is primary (e.g. Michael & Schilling, 1989). Glasses with anomalously high H_2O contents within a region, similar to sample 1568-2014, are also found in other areas of the mid-ocean ridge system. The origin for this sort of local variability is the subject matter of Part 2 of this study

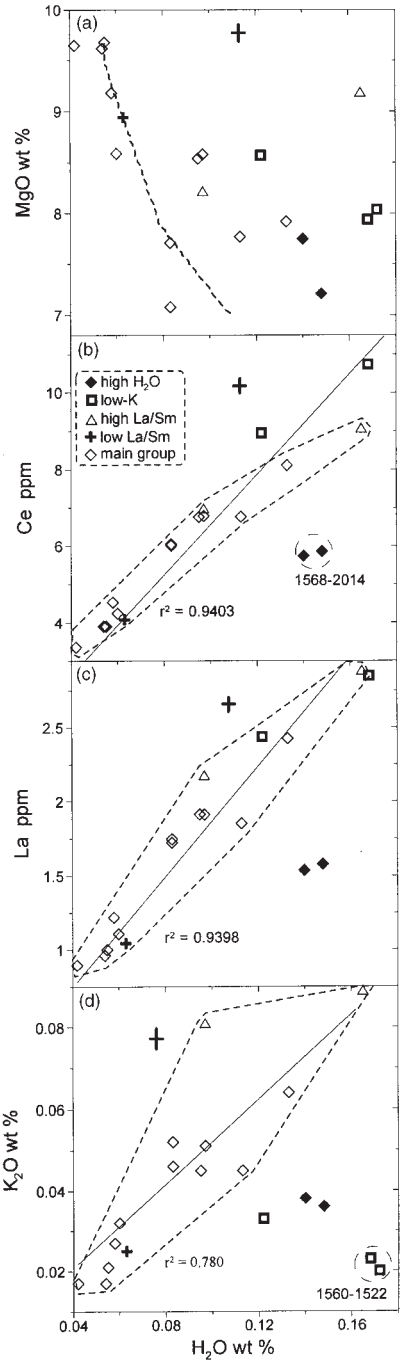

Fig. 2. H_2O contents of the Lamont Seamount glasses. High-H_2O glasses (two glass chips from sample 1568-2014) are defined in (b) and (c); low-K glasses (two glass chips from sample 1560-1522 and sample 1558-2014) are defined in (d); high-(La/Sm) and low-(La/Sm) glasses are defined in Fig. 4e; ◇, main group of Lamont Seamount glasses defined in Fig. 4e and g; dashed line in (a) shows crystallization path of the most magnesian glass, which was calculated at 10 MPa (see Appendix B for calculation details); continuous lines in (b)–(d) show least-squares linear best fits forced through the origin for glasses encompassed by dotted lines; correlation coefficients in (b)–(d) are for least-squared linear best fits not forced through the origin for the encompassed glasses. Analytical error bars are shown in all plots.

(Danyushevsky *et al.*, in preparation), and therefore this sample is not considered further in this paper.

The correlation between H_2O and K_2O in Lamont glasses is significantly worse than between H_2O and light REE (LREE) (Fig. 2d). Moreover, two samples, 1558-2014 and 1560-1522, have lower K_2O at a given H_2O than other samples (Fig. 2d). Analysis of the second glass chip from sample 1560-1522 confirms their anomalous characteristic (Table 1, Fig. 2d). Hereafter, we refer to these samples as the low-K group.

Other anomalies in compositions of the low-K samples

Trace-element contents of the studied glasses normalized to primitive mantle (Sun & McDonough, 1989) are shown in Fig. 3. Low-K samples are characterized by anomalous depletion, compared with other samples, in elements more incompatible than La. However, H_2O contents of these anomalous samples are not depleted and are consistent with other samples at a given LREE content (Fig. 2b and c). This results in higher H_2O/K_2O values [Fig. 2d, and also high H_2O/(Nb, Ba, or Rb) and LREE/(K_2O, Nb, Ba, or Rb), not shown in Fig. 2] of the low-K group samples compared with the rest of the Lamont glasses. The low-K samples also have the highest Sm/Yb values (Fig. 3), and lower La/Ce at a given $(La/Sm)_N$ (Fig. 5a, see below), indicating that La was also affected by the depletion event, although that cannot be clearly seen in Fig. 3. A possible origin of this anomalous geochemistry will be discussed below.

Variations in compositions of Lamont Seamount parental magmas

To minimize the effects of fractionation, we have recalculated the compositions of all glasses to 8 wt % MgO [see Klein & Langmuir (1987); see Appendix B for the recalculating procedure]. Olivine and plagioclase are the only phases assumed to have crystallized before quenching on the sea floor [see Allan *et al.* (1989) for rationale].

Recalculated major-element compositions are shown in Fig. 4a–d. In each of these plots, the glasses form relatively well-defined trends of normalized concentrations [such concentrations referred to hereafter as 'oxide(8)']. The large range of normalized concentrations reflects the diversity of parental magma major-element compositions. We have also recalculated a set of 148 Lamont Seamount glasses presented by Allan *et al.* (1989), which display similar trends and are shown in Fig. 4 for comparison.

We also note that a significant range of normalized concentrations exists on each seamount. The largest variation is observed on seamount MIB, where glass compositions range from the highest to very low $Na_2O(8)$.

Whereas major elements behave systematically in all glasses, trace-element patterns are more complex (Fig. 4e–h). Normalized La/Sm values (Fig. 4e) correlate with $Na_2O(8)$ in most samples (defined as the main group) but several glasses plot off the main group trend, with higher or lower $(La/Sm)_N(8)$ at a given $Na_2O(8)$. Glass $H_2O(8)$ and $K_2O(8)$ mimic the pattern shown by $(La/Sm)_N(8)$ (Fig. 4f and g), but samples anomalously depleted in strongly incompatible elements (low-K group, Figs 2d and 3) predictably have anomalously low $K_2O(8)$. The correlation between $H_2O(8)$ and $(La/Sm)_N(8)$ is shown in Fig. 14a (see below).

Thus, our analysis has identified four groups of Lamont Seamount parental magmas. The main group is characterized by covariations of major-element and incompatible-element contents. Compared with the main group, the high-(La/Sm) and low-(La/Sm) groups are enriched or depleted in incompatible elements at a given $Na_2O(8)$, respectively. The low-K group is anomalously depleted in strongly incompatible elements. However, variations in major elements are consistent in all four groups. We note that high- and low-(La/Sm) group samples have been described previously (Allan *et al.*, 1989; Niu & Batiza, 1991), but the low-K group is identified here for the first time.

Despite differences in geochemistry between the four groups, all Lamont Seamount magmas have constant $H_2O/La(8)$ [530 ± 50 (1σ), Fig. 5b]. Thus, $H_2O/Ce(8)$ is positively correlated with $(La/Sm)_N$ (Fig. 5c) in the same manner as La/Ce(8). As low-K samples have lower La/Ce(8) at a given $(La/Sm)_N(8)$, their $H_2O/Ce(8)$ values are also slightly lower (Fig. 5c). As expected (because K is more incompatible than La, e.g. Fig. 3), $H_2O/K_2O(8)$ decreases with increasing $(La/Sm)_N(8)$ (excluding the low-K group samples). These differences between H_2O/(La, Ce, and K_2O) behaviour can also be seen in Fig. 2, where the data points are scattered equally around the line passing through the origin in the H_2O–La plot (Fig. 2c), but form oblique trends in opposite directions in the H_2O–Ce and H_2O–K_2O plots (Fig. 2b and d).

To understand what controls H_2O geochemistry in Lamont Seamount lavas, we must consider their petrogenesis in more detail.

Can major-element variations in Lamont Seamount parental magmas reflect variable degrees of melting of a homogeneous mantle source?

The lack of a correlation between major- and trace-element contents in Lamont Seamount parental magmas, first described by Allan *et al.* (1989, fig. 15), was interpreted by those workers as reflecting a combination of trace-element source heterogeneity and variable degrees of melting (F) (see arrows in Fig. 4e). However, Allan *et al.* (1989) did not demonstrate that all major-element trends

Table 2: Trace element concentrations in the studied glasses

Sample:	R37-1	R38-1	R39-1	R41-1	R44-6	R46-2	R47-3	R48-1	R50-1	R51-1	R52-1	R56-5	R59-1	P2-3	P4-1	P22-1	P24-2	P59-2	P59-2	P64-3	P65-1	P66-2	P100-1
Region:	Zero-age 9·3–9·7°N EPR													Off-axis 9·5–11·3°N EPR									
Comments:	1,3	1,3	1,3	1,3	1,3	1,3	1,3	1,3	1,3	1,3	1,3	1,3	1,3	1,4	1,4	1,4	1,4	1,4	2	1,4	1,4	1,4	1,4
La	3·54	3·86	3·83	4·29	3·92	4·08	3·52	3·76	2·94	2·50	3·68	2·75	3·95	10·60	4·01	6·70	6·68	5·86	5·97	5·70	5·75	6·44	5·67
Ce	10·70	11·90	11·50	13·70	11·90	11·60	10·00	11·40	8·50	7·70	11·70	8·50	11·80	26·10	12·40	16·90	16·70	17·40	18·72	17·20	16·90	19·40	15·80
Nd	—	—	—	—	—	—	—	—	—	—	—	—	—	18·00	12·00	15·00	12·00	16·00	16·22	19·00	15·00	13·00	12·00
Sm	3·71	4·04	3·67	3·91	3·70	3·69	3·27	3·70	2·84	2·84	3·73	2·93	3·96	5·72	3·83	4·21	4·13	5·40	5·35	5·26	5·58	6·28	4·55
Eu	1·33	1·41	1·32	1·39	1·33	1·35	1·20	1·33	1·07	1·07	1·37	1·07	1·41	1·95	1·35	1·53	1·46	1·81	1·87	1·84	1·95	2·23	1·64
Gd	—	—	—	—	—	—	—	—	—	—	—	—	—	—	—	—	—	—	6·86	—	—	—	—
Tb	0·91	0·95	0·92	0·92	0·89	0·94	0·77	0·94	0·66	0·71	0·96	0·69	0·94	1·19	0·90	0·93	0·97	1·29	—	1·29	1·35	1·55	1·09
Dy	—	—	—	—	—	—	—	—	—	—	—	—	—	—	—	—	—	—	8·12	—	—	—	—
Er	—	—	—	—	—	—	—	—	—	—	—	—	—	—	—	—	—	—	5·08	—	—	—	—
Yb	3·41	3·74	3·42	3·50	3·48	3·55	3·10	3·56	2·64	2·71	3·58	2·76	3·75	4·23	3·63	3·35	3·40	4·96	4·84	4·82	5·18	5·86	4·00
Lu	—	—	—	—	—	—	—	—	—	—	—	—	—	—	—	—	—	—	0·728	—	—	—	—
Rb	—	—	—	—	—	—	—	—	—	—	—	—	—	—	—	—	—	—	2·449	—	—	—	—
Ba	—	—	—	—	—	—	—	—	—	—	—	—	—	—	—	—	—	—	21·149	—	—	—	—
Sr	—	—	—	—	—	—	—	—	—	—	—	—	—	—	—	—	—	—	118·9	—	—	—	—
Nb	—	—	—	—	—	—	—	—	—	—	—	—	—	—	—	—	—	—	5·41	—	—	—	—
Ta	—	—	—	—	—	—	—	—	—	—	—	—	—	—	—	—	—	—	0·349	—	—	—	—
Zr	—	—	—	—	—	—	—	—	—	—	—	—	—	—	—	—	—	—	147·9	—	—	—	—
Hf	—	—	—	—	—	—	—	—	—	—	—	—	—	—	—	—	—	—	3·98	—	—	—	—
Y	—	—	—	—	—	—	—	—	—	—	—	—	—	—	—	—	—	—	46·8	—	—	—	—
Th	—	—	—	—	—	—	—	—	—	—	—	—	—	—	—	—	—	—	0·297	—	—	—	—
U	—	—	—	—	—	—	—	—	—	—	—	—	—	—	—	—	—	—	0·126	—	—	—	—
Li	—	—	—	—	—	—	—	—	—	—	—	—	—	—	—	—	—	—	9·40	—	—	—	—
Be	—	—	—	—	—	—	—	—	—	—	—	—	—	—	—	—	—	—	0·75	—	—	—	—
B	—	—	—	—	—	—	—	—	—	—	—	—	—	—	—	—	—	—	2·59	—	—	—	—
Sc	—	—	—	—	—	—	—	—	—	—	—	—	—	—	—	—	—	—	41·5	—	—	—	—
V	—	—	—	—	—	—	—	—	—	—	—	—	—	—	—	—	—	—	445·0	—	—	—	—
Ga	—	—	—	—	—	—	—	—	—	—	—	—	—	—	—	—	—	—	20·5	—	—	—	—

Table 2: continued

Sample:	P100-1	P101-1	P102-1	P103-1	P104-1	P108-1	P109-1	P109-1	F1-1	F2	F2-1	F3-4	1558-1657	1558-2014	1571-1936	F9-1	1564-1857	1562-2112	1570-1830	1572-1727
Region:	Off-axis 9·5–11·3°N EPR								Lamont Seamounts											
Comments:	2	1,4	1,4	1,4	1,4	1,4	1,4	2	2	2	2	2	2	2	2	2	2	2	2	2
La	5·77	5·78	5·03	4·83	5·59	10·49	4·72	4·70	2·18	0·96	1·00	0·90	1·11	2·44	2·42	2·89	1·22	1·85	1·04	1·91
Ce	17·72	16·70	14·00	14·90	15·60	25·60	13·70	14·25	6·99	3·91	3·90	3·36	4·24	8·95	8·11	9·09	4·53	6·77	4·08	6·78
Nd	14·44	14·00	12·00	11·00	14·00	16·00	10·00	11·27	6·89	4·62	4·60	4·28	5·07	8·61	8·71	7·96	5·09	7·49	5·22	7·21
Sm	4·62	4·67	4·31	4·13	4·24	4·88	3·58	3·50	2·57	1·80	1·87	1·85	2·01	2·83	3·16	2·63	2·07	2·89	2·18	2·64
Eu	1·67	1·73	1·52	1·53	1·48	1·68	1·32	1·36	1·01	0·77	0·78	0·74	0·86	1·16	1·26	1·07	0·83	1·11	0·88	1·05
Gd	5·76	—	—	—	—	—	—	4·32	3·62	2·73	2·73	2·74	3·15	3·92	4·34	3·65	3·08	4·04	3·18	3·67
Tb	—	1·09	0·99	1·02	0·97	0·97	0·80	—	—	—	—	—	—	—	—	—	—	—	—	—
Dy	6·72	—	—	—	—	—	—	4·84	4·47	3·42	3·39	3·44	4·07	4·48	5·11	4·20	3·82	5·00	4·03	4·40
Er	4·12	—	—	—	—	—	—	2·94	2·82	2·19	2·17	2·22	2·59	2·83	3·13	2·61	2·39	3·16	2·54	2·78
Yb	3·95	4·01	3·64	3·66	3·64	3·25	2·81	2·75	2·65	2·07	2·02	2·05	2·52	2·53	2·85	2·48	2·21	2·94	2·41	2·55
Lu	0·590	—	—	—	—	—	—	0·411	0·408	0·307	0·322	0·327	0·371	0·398	0·451	0·397	0·342	0·464	0·360	0·397
Rb	2·430	—	—	—	—	—	—	2·064	0·497	0·141	0·143	0·195	0·253	0·108	0·541	0·558	0·191	0·335	0·272	0·453
Ba	22·529	—	—	—	—	—	—	22·690	4·663	1·501	1·533	1·846	2·350	1·829	5·393	5·530	2·591	3·003	2·291	4·895
Sr	156·1	—	—	—	—	—	—	187·5	109·9	90·0	90·7	79·8	79·3	171·3	132·8	167·5	94·2	111·1	86·0	125·0
Nb	5·24	—	—	—	—	—	—	4·30	1·40	0·42	0·40	0·52	0·60	0·65	1·50	1·70	0·74	0·95	0·58	1·06
Ta	0·339	—	—	—	—	—	—	0·272	0·100	0·026	0·028	0·036	0·040	0·056	0·108	0·115	0·048	0·067	0·040	0·069
Zr	128·4	—	—	—	—	—	—	98·3	61·6	40·2	40·5	35·8	43·1	81·7	75·6	78·3	44·3	66·9	43·0	62·6
Hf	3·40	—	—	—	—	—	—	2·52	1·86	1·31	1·31	1·26	1·43	2·25	2·30	2·12	1·44	2·13	1·50	1·93
Y	37·8	—	—	—	—	—	—	26·8	25·6	19·7	19·7	20·1	23·8	25·0	28·4	24·3	21·5	28·4	23·1	25·0
Th	0·294	—	—	—	—	—	—	0·248	0·083	0·022	0·020	0·020	0·031	0·048	0·078	0·097	0·034	0·044	0·030	0·063
U	0·124	—	—	—	—	—	—	0·104	0·040	0·008	0·008	0·010	0·015	0·021	0·043	0·043	0·020	0·029	0·019	0·027
Li	7·64	—	—	—	—	—	—	5·83	—	—	—	—	—	—	—	—	—	—	—	—
Be	0·70	—	—	—	—	—	—	0·58	—	—	—	—	—	—	—	—	—	—	—	—
B	1·60	—	—	—	—	—	—	1·50	—	—	—	—	—	—	—	—	—	—	—	—
Sc	41·8	—	—	—	—	—	—	36·8	41·8	33·5	32·8	32·9	41·1	35·5	40·9	36·4	36·3	44·2	36·0	36·7
V	381·9	—	—	—	—	—	—	280·9	281·6	211·4	207·0	217·2	264·6	227·3	264·6	236·1	228·8	284·4	231·3	238·8
Ga	19·6	—	—	—	—	—	—	18·4	16·9	16·0	15·6	15·9	17·0	17·0	17·5	16·8	16·7	17·2	16·5	17·2

Table 2: continued

Sample:	1572-1755	1560-1651	1560-1522/2	1568-2014/1	1568-2014/2	1569-1601	1-1	1-2	10-10	11-9	13-20	16-28	16-9	19-54	3-2	9-14	9-17	16-12	16-2	17-1	17-18
Region:	Lamont Seamounts						127–129°E SEIR														
Comments:	2	2	2	2	2	2	2	2	2	2	2	2	2	2	2	2	2	2	2	2	2
La	1·91	1·72	2·85	1·58	1·57	1·75	5·08	4·76	5·92	3·35	4·77	2·97	2·87	5·39	6·42	4·10	3·67	6·15	5·97	1·93	1·92
Ce	6·76	6·05	10·73	5·90	5·82	6·01	18·30	17·46	19·84	13·46	18·29	10·10	10·24	18·94	23·42	15·19	14·57	17·20	17·22	7·60	7·75
Nd	7·15	6·49	10·13	6·87	6·69	6·34	16·89	16·30	19·60	12·52	16·56	10·24	9·92	17·55	21·84	14·28	12·94	13·45	13·01	8·13	8·11
Sm	2·68	2·53	3·38	2·63	2·57	2·48	5·78	5·66	6·63	4·31	5·65	3·45	3·37	5·90	7·37	4·82	4·36	3·96	3·79	2·92	2·87
Eu	1·05	0·99	1·25	1·06	1·02	0·99	1·93	1·92	2·16	1·60	1·95	1·32	1·31	2·03	2·41	1·69	1·56	1·47	1·43	1·16	1·15
Gd	3·73	3·63	4·37	3·87	3·78	3·75	7·50	7·34	8·62	5·54	7·24	4·46	4·33	7·59	9·62	6·24	5·33	4·86	4·55	3·86	3·77
Tb	—	—	—	—	—	—	—	—	—	—	—	—	—	—	—	—	—	—	—	—	—
Dy	4·46	4·49	5·02	4·79	4·67	4·67	9·01	8·87	10·35	6·54	8·60	5·40	5·11	9·13	11·45	7·34	6·22	5·56	5·14	4·72	4·53
Er	2·74	2·79	3·03	3·01	2·90	3·00	5·61	5·53	6·43	4·05	5·35	3·27	3·10	5·62	7·21	4·51	3·83	3·32	3·08	2·86	2·81
Yb	2·56	2·66	2·75	2·87	2·77	2·84	5·41	5·28	6·19	3·90	5·16	3·11	2·99	5·50	6·91	4·31	3·69	3·15	2·94	2·77	2·69
Lu	0·387	0·408	0·423	0·434	0·417	0·435	0·817	0·794	0·920	0·577	0·779	0·461	0·442	0·794	1·051	0·646	0·545	0·465	0·431	0·409	0·398
Rb	0·456	0·378	0·134	0·309	0·310	0·379	1·286	1·020	0·907	0·491	1·022	0·348	0·361	1·035	1·320	0·663	0·661	0·918	0·912	0·180	0·185
Ba	4·879	3·360	1·181	2·813	2·780	3·687	11·183	8·234	7·301	3·962	8·406	3·558	3·600	8·273	10·307	5·335	5·120	8·407	8·364	1·754	1·766
Sr	125·6	103·3	195·2	95·6	95·0	89·2	104·4	98·5	122·8	108·7	99·0	137·9	139·0	118·6	102·3	115·3	112·1	229·0	227·9	103·4	103·9
Nb	1·03	0·97	0·43	0·80	0·80	1·00	2·71	2·43	2·80	1·40	2·47	1·26	1·25	3·06	3·33	1·86	1·80	4·10	4·10	0·71	0·69
Ta	0·067	0·071	0·048	0·056	0·054	0·068	0·201	0·182	0·224	0·106	0·181	0·098	0·098	0·223	0·245	0·141	0·123	0·304	0·283	0·060	0·056
Zr	62·8	58·4	96·6	59·9	59·6	57·4	159·2	154·0	197·1	107·8	147·1	95·8	91·6	166·9	212·1	132·3	115·7	138·5	132·6	70·9	69·3
Hf	1·94	1·79	2·60	1·91	1·83	1·78	4·47	4·31	5·49	3·13	4·17	2·59	2·52	4·64	5·89	3·68	3·06	3·30	3·07	2·13	2·07
Y	25·0	25·7	27·6	27·7	27·5	27·6	50·4	49·8	57·2	35·9	47·5	29·6	28·2	49·9	65·5	40·7	35·6	30·1	28·8	25·7	25·0
Th	0·061	0·047	0·033	0·043	0·041	0·051	0·152	0·136	0·176	0·079	0·134	0·074	0·068	0·164	0·190	0·110	0·093	0·232	0·217	0·042	0·039
U	0·030	0·048	0·023	0·021	0·020	0·026	0·082	0·074	0·084	0·048	0·078	0·033	0·035	0·090	0·102	0·057	0·054	0·111	0·108	0·022	0·021
Li	—	—	—	—	—	—	9·50	9·67	8·77	8·34	9·96	5·68	5·97	9·09	12·31	8·18	7·70	5·31	5·24	5·55	5·65
Be	—	—	—	—	—	—	0·71	0·67	0·78	0·47	0·71	0·52	0·42	0·76	0·87	0·54	0·56	0·83	0·81	0·33	0·32
B	—	—	—	—	—	—	2·08	2·46	2·20	1·81	2·25	1·34	1·46	2·35	2·79	1·86	1·82	1·90	2·02	1·16	1·11
Sc	36·8	41·9	37·5	44·2	44·4	45·3	38·9	40·4	41·8	35·9	37·8	39·8	37·9	39·4	40·0	38·0	35·4	34·9	33·7	34·5	33·8
V	236·3	268·4	235·1	284·8	285·3	310·9	436·0	436·0	382·7	353·1	448·2	257·0	261·0	411·2	528·1	353·4	360·3	243·9	248·5	248·7	256·8
Ga	17·1	17·5	16·9	17·0	17·2	17·3	20·0	19·9	19·1	19·0	20·6	16·8	17·2	19·9	22·8	18·8	19·5	17·2	17·6	16·3	17·0

Concentrations in ppm; 1, REE by INAA; 2, REE by LA-ICP-MS; 3, REE from Batiza & Niu (1992); 4, REE from R. Batiza (unpublished data, 1996).

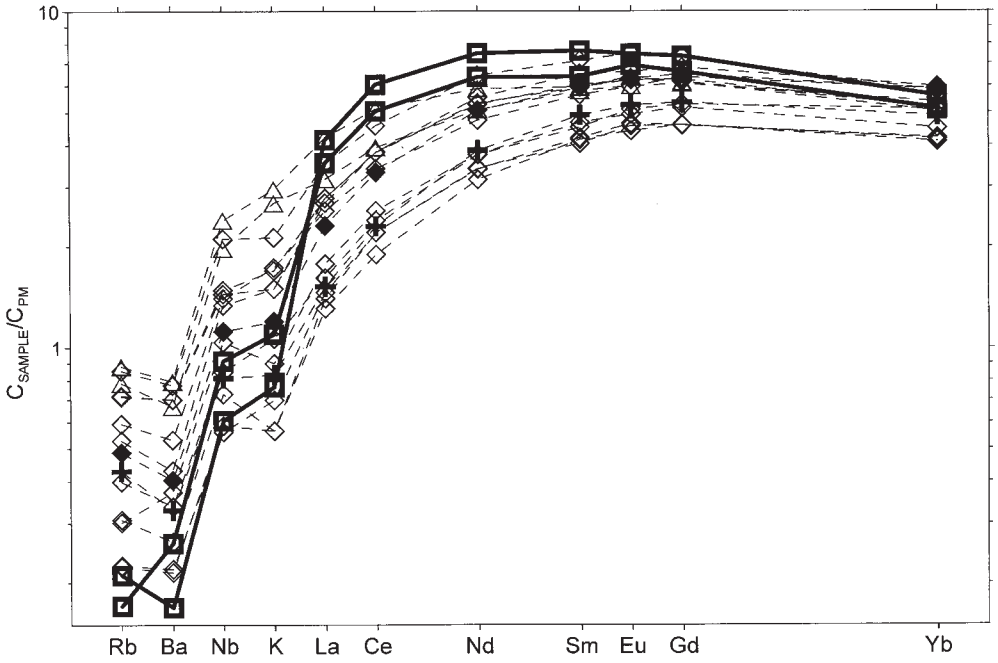

Fig. 3. Trace-element contents in the Lamont Seamount glasses normalized to the primitive mantle (PM) (Sun & McDonough, 1989). Symbols as in Fig. 2. Glasses from the low-K_2O group (□) are characterized by anomalous depletion in elements more incompatible than La.

(Fig. 4a–d) are consistent with variable degrees of melting of a single source. Alternatively, such trends may reflect mixing of magmas produced from lithologically heterogeneous mantle (e.g. harzburgite vs lherzolite) as suggested by Natland (1989).

Niu & Batiza (1991) suggested that Lamont Seamount magmas are erupted simultaneously at different distances from the ridge crest, and that variations in their major-element compositions thus reflect the variable length of the melting columns under seamounts, which decreases away from the ridge (Batiza *et al.*, 1990). In contrast, Lundstrom *et al.* (1999) argued that Lamont Seamount magmas are erupted over a >600 ky time interval at a constant distance from the ridge crest, which reflects the position of a vertical dunite melt conduit within a broader melting regime.

To evaluate whether major-element trends of the Lamont Seamount glasses (Fig. 4a–d) reflect variable F of a mantle source, we have compared them with the results of high-P mantle-melting experiments (Fig. 6). For this comparison we have chosen experiments performed at the University of Tasmania (Falloon *et al.*, 1997, 1999, 2000) and at the University of Bristol (Robinson *et al.*, 1998), as those were carried out on appropriate mantle source compositions, have demonstrated equilibrium, reported large ranges of F, and have consistent T measurements. Differences between these experiments and experiments of Kinzler & Grove (1992), Baker *et al.* (1995), and Kinzler (1997) were discussed by Falloon *et al.* (1997, 1999, 2000).

It is important to note that experimentally studied peridotite compositions differ in *mg*-number [100Mg/(Mg + Fe)]. Higher *mg*-number of a starting composition results in lower FeO and higher SiO_2 contents of a partial melt at a given T and P. The studied peridotite compositions cover a wide range of *mg*-number: MORB pyrolite with *mg*-number = 92 [MPY-92, Robinson *et al.* (1998)]; Tinaquillo lherzolite with *mg*-number = 90 [TQ-90, Robinson *et al.* (1998)]; MPY-87, TQ-88·5, and MM3-90·5 (Falloon *et al.*, 1997, 1999, 2000). The starting compositions also differ in their fertility (i.e. the proportion of the basaltic component, which can be measured either by the normative amount of nepheline, plagioclase, and diopside, or by the concentrations of Na_2O, Al_2O_3, and CaO). The latter differences result in variable F at a given T and P. Among studied compositions, MPY-92 is the most fertile, followed by MPY-87, MM3-90·5, and TQ (studied compositions of TQ-88·5 and TQ-90 have similar fertility).

As the compositions of primary magmas for the Lamont Seamounts (i.e. the compositions of melts that were in equilibrium with the mantle) are not known, we have recalculated experimental melt compositions to 8 wt % MgO (see Niu & Batiza, 1991) (Fig. 6; see Appendix B for calculating procedure).

The importance of melt H_2O contents for comparing MORB magmas with anhydrous peridotite-melting experiments. Figure 6a shows recalculated compositions of anhydrous mantle

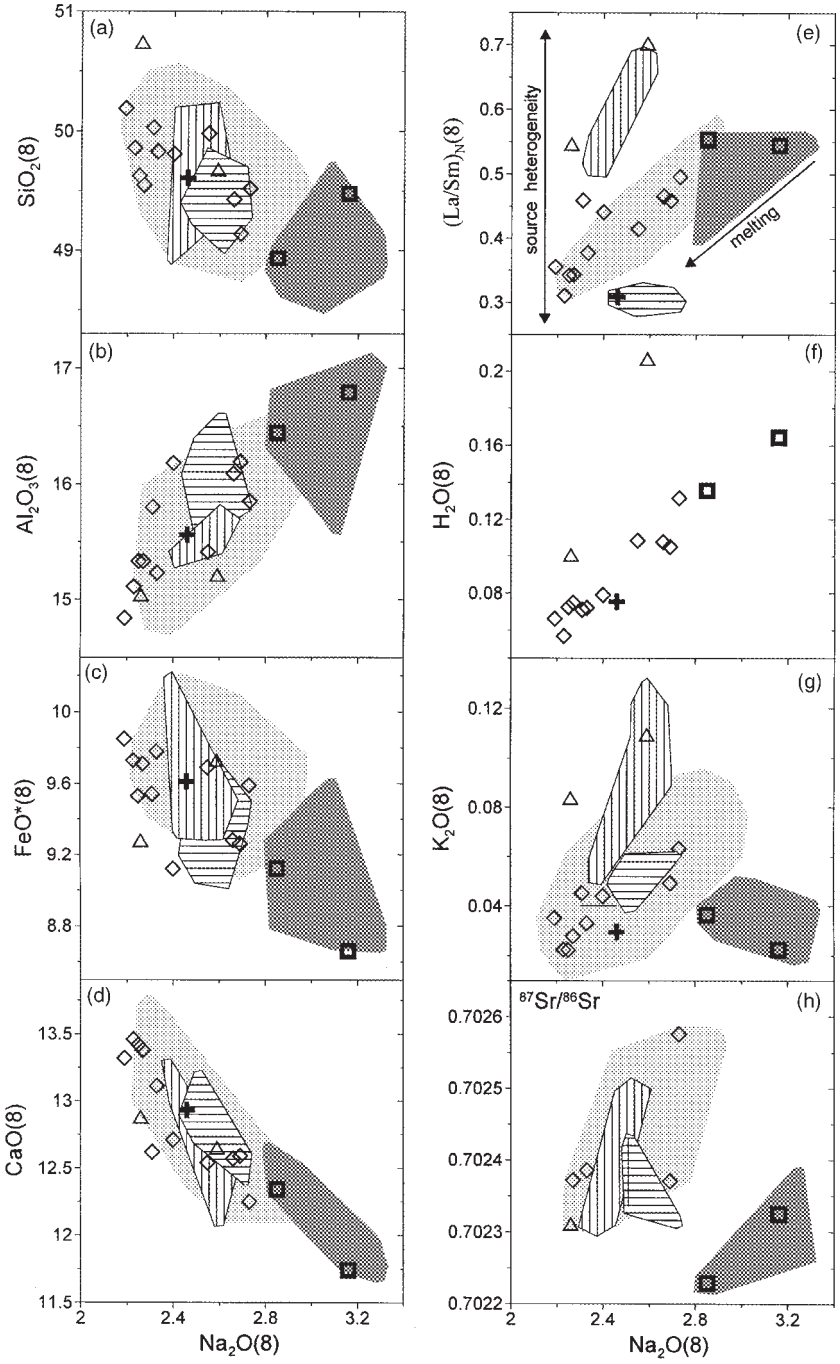

Fig. 4. Compositions of the Lamont Seamount glasses recalculated to 8 wt % MgO. Symbols as in Fig. 2. Low-La/Sm (sample 1570-1830) and high-La/Sm (samples F9-1 and F1-1) glasses are defined in (e) as plotting below or above the trend defined by the main group (◇); fields show 148 Lamont Seamount glasses analysed by Allan *et al.* (1989). The dataset of Allan *et al.* (1989) (light grey field shows the main group) conforms to the same four groups as our dataset. Low-La/Sm glasses (horizontally striped field) were found on seamount MOK only, dives 1570 and 1561 (14 samples); high-La/Sm glasses (vertically striped field) were found on cones of seamounts MOK and SASHA, dredges 9, 1, 11 (11 samples); low-K_2O glasses (dark grey field) were found on seamounts DTD (dive 1572; two samples), MIB (dives 1559, 1560; six samples), MOK (1563, 1564; two samples), and SASHA (1558; five samples). Observed differences in K_2O contents (g) of some glasses analysed in this study and by Allan *et al.* (1989) are probably caused by the shorter counting times during electron microprobe analyses used by Allen *et al.* (1989). Arrows in (e) show the interpretation of the compositional diversity of the Lamont Seamount glasses by Allan *et al.* (1989). In (e), normalization to primitive mantle of Sun & McDonough (1989). $^{87}Sr/^{86}Sr$ values are from Fornari *et al.* (1988).

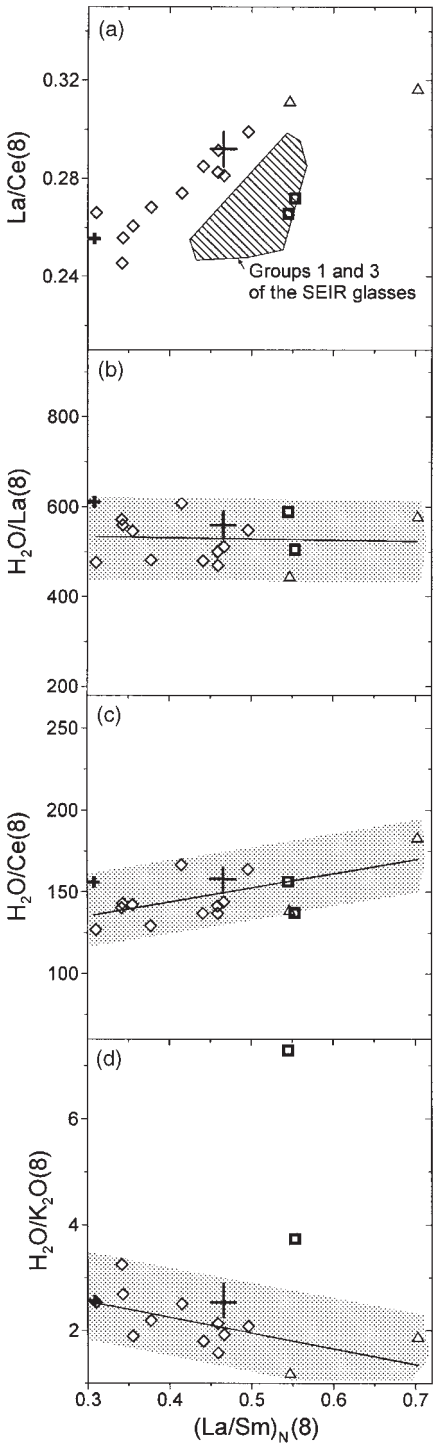

Fig. 5. Relative H_2O contents of the Lamont Seamount glasses. Symbols as in Fig. 2. The scale for each *y*-axis is chosen so that the size of error bars (shown as cross in each plot) is approximately similar for *y*- and *x*-axes in each plot. La/Ce(8) of the SEIR glasses from Groups 1 and 3 are shown for comparison in (a). (See text for discussion on regional differences between the ERP and SEIR glasses.) Normalization to primitive mantle of Sun & McDonough (1989).

melts fractionated at low *P* (see Appendix B for recalculation procedure). Despite compositional differences between starting compositions discussed above, all melts define a narrow trend in $Al_2O_3(8)$–$Na_2O(8)$ space that is oblique to that defined by the Lamont Seamount glasses, and shifted towards lower $Al_2O_3(8)$. The observed shift reflects the presence of H_2O in natural magmas that suppresses plagioclase crystallization and significantly affects the liquid line of descent, even at low H_2O concentrations (see Appendix B for more details). A larger difference between Lamont glasses and anhydrous melts at higher $Na_2O(8)$ reflects a positive correlation between $H_2O(8)$ and $Na_2O(8)$ in the Lamont Seamount glasses (Fig. 4f).

To allow a comparison between the Lamont Seamount glasses and experimental melts, we recalculated the latter to 8 wt % MgO assuming some H_2O in the melt. Small amounts of H_2O (<0·4 wt % in the melt) will cause some increase in *F* at given *T* and *P*, but should not significantly displace melt compositions from the anhydrous olivine + orthopyroxene + clinopyroxene cotectics (e.g. Danyushevsky *et al.*, 1994; Falloon & Danyushevsky, 2000). For the comparative purposes of our study, we ignored the difference in *F* between perfectly anhydrous and slightly 'wet' conditions. We also note that melts in nominally anhydrous mantle melting experiments may contain up to 0·2 wt % H_2O (L. V. Danyushevsky & T. J. Falloon, unpublished data, 1999), which makes this difference in *F* negligible.

We used the following iterative procedure to estimate H_2O contents of the experimental melts, which are required to allow a comparison between them and the Lamont Seamount glasses: (1) we choose an arbitrary H_2O content for each studied peridotite composition (e.g. 200 ppm); (2) the H_2O content in each experimental liquid is then calculated from the H_2O content of its source peridotite using *F* of that particular experiment, and assuming a bulk H_2O distribution coefficient (K_d) of 0·01; (3) melt compositions are then recalculated to 8 wt % MgO; (4) if the new trend for a starting peridotite composition is below (or above) the field of Lamont Seamount glasses in Fig. 6a, then melts from this peridotite are recalculated using a higher (or lower) source H_2O content. These steps are repeated until the trends of recalculated experimental melts pass through the field of the Lamont Seamount glasses (Fig. 6a). Source H_2O contents for each peridotite that produced the best fit between Lamont Seamount glasses and recalculated mantle melts (264 ppm for TQ; 308 ppm for MM3-90·5; 485 ppm for MPY-87; 517 ppm for MPY-92) are within the range of MORB mantle source (~100–450; see Introduction).

Despite significant differences in starting compositions, the observed trends of $SiO_2(8)$, FeO*(8), and CaO(8) vs $Na_2O(8)$ for experimental melts are clearly subparallel at

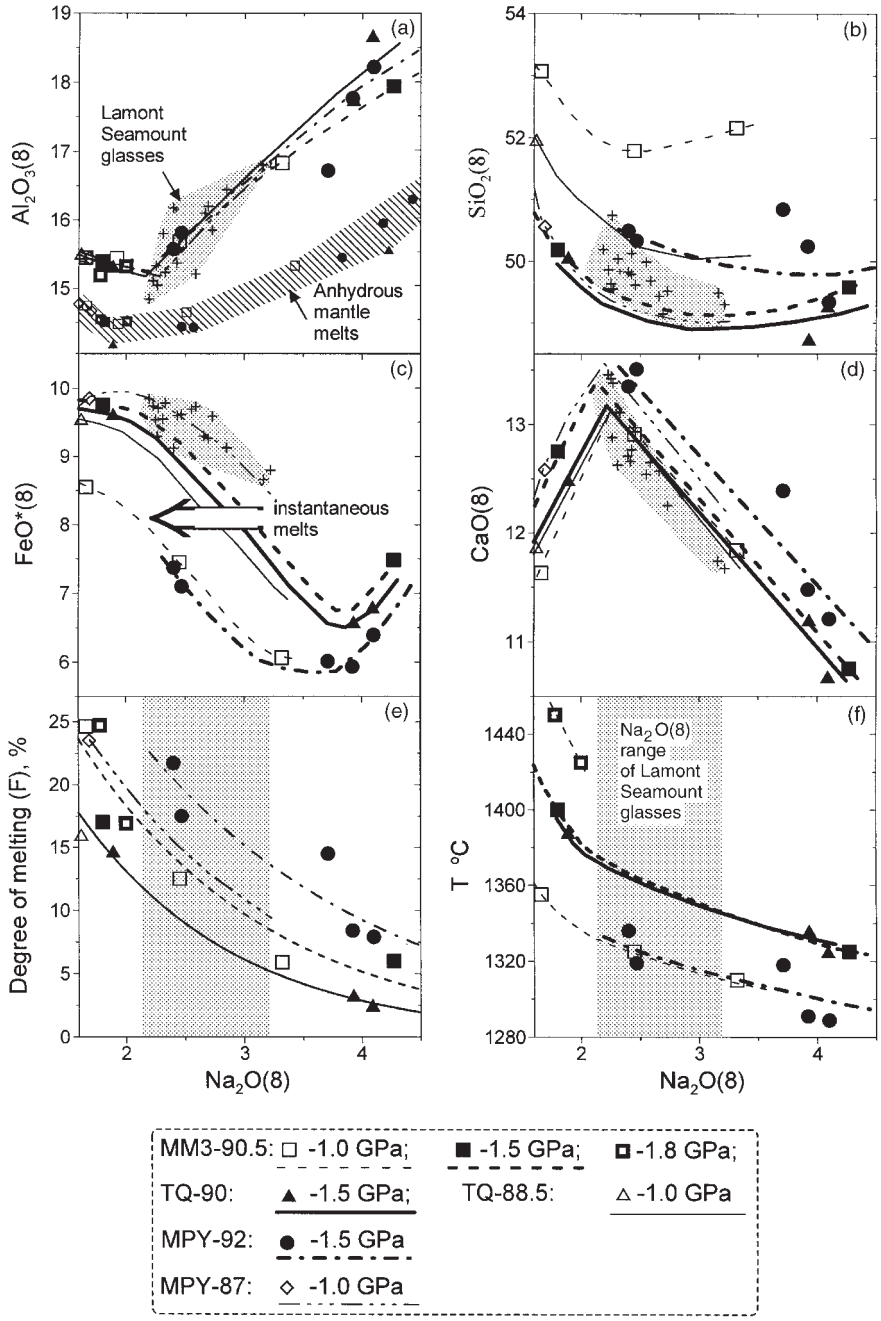

Fig. 6. Comparison between Lamont Seamount glasses and liquids produced in high-*P* peridotite melting experiments. All compositions are recalculated to 8 wt % MgO as described in the text and Appendix B. Grey field in Fig. 6a–d shows compositions of the Lamont Seamount glasses. Individual analyses are shown as small crosses. Grey column in Fig. 6e and f shows the range of $Na_2O(8)$ in the Lamont Seamount glasses, as the degree of melting and source-mantle *T* for Lamont Seamount magmas are unknown. Squares, partial melts produced in experiments with MM3-90·5 starting composition (numbers following the abbreviation represent *mg*-number of the starting composition); triangles, partial melts produced in experiments with TQ-90 and TQ-88·5 starting compositions; dots, partial melts produced in experiments with MPY-92 starting composition; diamonds, partial melts produced in experiments with MPY-87 starting composition. Small symbols in Fig. 6a represent experimental melts recalculated to 8 wt % MgO under anhydrous conditions. Large symbols represent experimental melts recalculated to 8 wt % MgO assuming small amounts of H_2O in the source. (See text for detailed description of how source H_2O contents were estimated.) Experiments at 1·0 and 1·5 GPa with a single starting composition are approximated by lines with the same pattern but variable thickness in Fig. 6b–d and f, as shown in the legend. Experiments at 1·8 GPa with MM3-90·5 are shown in Fig. 6e and f only. Large arrow in (c) show general direction of the change in compositions of instantaneous melts produced in a melting column.

10 and 1·5 GPa (Fig. 6b–d). For a given mantle composition (e.g. MM3-90·5), 1·5 GPa melts are significantly higher in FeO*(8) and lower in SiO_2(8) at a given Na_2O(8) than are 1·0 GPa melts, consistent with conclusions of Niu & Batiza (1991), who used FeO*(8)/SiO_2(8) as an indicator of melting *P*. Major-element trends defined by Lamont Seamount glasses are in general consistent with the trends formed by experimental melts (Fig. 6a–d), and as can be seen in the plot with FeO especially, they resemble liquids separated from their source over a limited range of *P*.

Another important observation is that melts from variably fertile mantle sources form sub-parallel trends in an *F*–Na_2O(8) diagram (Fig. 6e). The data are insufficient to estimate whether Na_2O(8) depends on *P* at a given *F* for a given mantle composition. However, available data for MM3-90·5 between 1·0 and 1·8 GPa suggest that variations in the mantle composition exert the major control, consistent with conclusions of Niu & Batiza (1991). Thus, if the Lamont magmas originated by various *F* from mantle sources with similar major-element compositions, the difference between the smallest and the largest *F* was 7–10%, regardless of the initial fertility of the source and the actual value of *F*.

Is it possible to constrain the melting mechanism? If we assume that individual Lamont Seamount magmas represent instantaneous melts separated at various depths from a melting column, the difference in *P* between magmas formed at the lowest and the highest *F* is >0·5 GPa [using melting rate estimates of Langmuir *et al.* (1992) and Reynolds & Langmuir (1997)]. A minimum 0·5 GPa difference in the *P* of melting is not consistent with the data, as the combined effect of progressively decreasing *P* and increasing *mg*-number of the source prevents an increase in FeO*(8) in instantaneous melts with increasing *F* [decreasing Na_2O(8), Fig. 6c]. Nearly constant FeO*(8) in instantaneous melts produced at >5% total melting were also inferred by Langmuir *et al.* (1992, fig. 60). Thus Lamont Seamount glasses cannot represent instantaneous melts from a melting column, consistent with conclusions of Niu & Batiza (1991).

Lamont Seamount magmas can represent relatively high-*F* batch melts separated at similar *P* from a series of small mantle diapirs of similar major-element compositions, that were characterized by variable initial T (variable initiation depths?) and thus experienced different *F*. As follows from Fig. 6f, the difference in T between the highest and the lowest *F* must be ~25°C, regardless of the separation *P* and source fertility.

Alternatively, Niu & Batiza (1991) suggested that Lamont Seamount glasses represent accumulated melts from melting columns beneath each seamount. However, this hypothesis cannot readily account for the range of Na_2O(8) (and thus *F*) found on each seamount. Another scenario has been offered by Lundstrom *et al.* (1999), who proposed that seamount formation results from focusing of melts from a wider melting regime to a specific off-axis location.

Summary. Although the exact melting mechanism in the mantle beneath Lamont Seamounts is arguable, we can conclude that variations in major-element contents in Lamont parental magmas are consistent with variable degrees of melting of a relatively homogeneous (in terms of major elements) mantle source. This also allows an estimation of the contribution of variations in *F* to the range of $(La/Sm)_N$(8). Indeed, a positive correlation between Na_2O(8) and $(La/Sm)_N$(8) displayed by the main and low-K groups of Lamont glasses (Fig. 4e) suggests that their range of $(La/Sm)_N$(8) (~0·3–0·55) reflects variable *F*. Using a set of K_d values and melting reactions, Allan *et al.* (1989, fig. 18) demonstrated a similar relationship between *F* and $(La/Sm)_N$ for total degrees of melting >5%. We will use this estimation when describing other glass suites for which an estimation of variations in *F* is not possible.

Origin of variations in incompatible elements

It has been suggested (e.g. Zindler *et al.*, 1984; Niu *et al.*, 1996; Niu & Batiza, 1997; Lundstrom *et al.*, 1999) that mantle beneath the EPR is composed of two physically distinct components, with the enriched component forming veins or 'plums' of variable sizes distributed in the more depleted peridotite matrix. When magma is formed during melting of such two-component mantle, early-stage low-*F* melts contain high proportions of the enriched component with elevated abundances of incompatible elements, high La/Sm, and more radiogenic Sr isotopes. Indeed, there are many areas along the EPR whose samples fit this model very well.

However, this model cannot explain compositional variations of Lamont Seamount magmas, as can be seen clearly in Fig. 4. Glasses from the high-La/Sm group do not have higher $^{87}Sr/^{86}Sr$ than glasses from the main group (Fig. 4h). This implies that enrichment in incompatible elements in the source of these magmas was contemporaneous (much less than the half-life of ^{87}Rb) with magma genesis. Moreover, major-element characteristics of high-La/Sm glasses are not consistent with low *F*. On the contrary, some of these glasses have very low Na_2O(8) (Fig. 4e) and Al_2O_3(8) (Fig. 4b), and high CaO(8) (Fig. 4d) and CaO/Al_2O_3 values, indicating high *F*. All this is inconsistent with the long-lived separate enriched domains as the source of high-La/Sm Lamont glasses.

On the other hand, glasses anomalously depleted in strongly incompatible elements (low-K group) have had low Rb/Sr values for a long enough time to be reflected

by $^{87}Sr/^{86}Sr$. However, major elements in these glasses indicate the smallest F among Lamont magmas (Fig. 4a–d), and thus these low $^{87}Sr/^{86}Sr$ magmas cannot represent the depleted peridotite matrix.

Allan *et al.* (1989) suggested that major-element-independent variations of incompatible elements may be explained if Lamont Seamount magmas represent near-solidus (low F) melts separated from their sources around the depths of the spinel–plagioclase transition (0·8–1·0 GPa). The variable lithology of the mantle in this case would cause differences in incompatible-element contents as a result of changing bulk K_d values, whereas major elements will be less affected. This explanation appears unlikely, however, as glasses from both high- and low-La/Sm groups reflect significant F (>10%, Fig. 6), whereas plagioclase is exhausted in the residue of melting at significantly lower F (e.g. Falloon *et al.*, 1999).

Probably, compositions of glasses with higher and lower $(La/Sm)_N(8)$ compared with the main group at a given $Na_2O(8)$ reflect complex patterns of melt redistribution during melting (either within a diapir, or within a melting column), similar to the conclusions of Niu & Batiza (1991) [see also Niu *et al.* (1996) for a detailed discussion].

Magmas anomalously depleted in strongly incompatible elements (low-K group, Figs 2 and 3) were probably formed from a source previously depleted by the separation of a small melt fraction. This depletion did not affect the relative proportions between elements more compatible than La, or the effect was not large enough to be seen through the next melting event during formation of Lamont Seamounts. Unlike glasses from the low-La/Sm group, low-K magmas have anomalously low $^{87}Sr/^{86}Sr$ (compared with the main group) (Fig. 4h), suggesting that this previous melting occurred at a substantial time interval before the melting event that formed Lamont Seamounts, and does not represent melt redistribution. Rather, it reflects long-established source heterogeneity.

Summary

The origin of Lamont Seamount magmas involved complex processes such as melting to variable F of a source that was heterogeneous in strongly incompatible elements and subsequent melt redistribution within the melting region. An important result of our analysis is that despite the variety of different processes involved in the evolution of the Lamont Seamount mantle source before and during production of the Lamont Seamount magmas, the behaviour of H_2O mimics that of La (Fig. 5).

Normal crust samples between 9·3°N and 11·3°N

Ridge-crest samples between 9·3 and 9·7°N are typical NMORB [$0·55 < (La/Sm)_N < 0·72$] and cover an MgO range from 6·7 to 8·4 wt % (Batiza & Niu, 1992). La/Sm and K_2O/TiO_2 values appear to increase slightly with decreasing MgO; however, the correlations are rather poor and scattered and are not considered significant (Batiza & Niu, 1992). Normal crust samples from off-axis locations at 9·5°N, 10·5°N and 11·3°N are generally more evolved than the ridge-crest samples (MgO ~ 4·5–7·5 wt %) and are relatively enriched in incompatible elements $0·65 < (La/Sm)_N < 1·4$ (Batiza *et al.*, 1996; Niu *et al.*, 1999; Regelous *et al.*, 1999). Strongly incompatible element contents and their ratios show significant variations at a given MgO, reflecting involvement of processes other than crystallization in their petrogenesis.

Compositions of glasses analysed in this study are presented in Tables 1 and 2. The H_2O contents generally increase with decreasing MgO, but display significant variations at a given MgO. As in the case with the Lamont Seamount glasses, good positive correlations exist between H_2O and K, La, or Ce contents for all samples (excluding the set from 10·5°N, which has a limited compositional range) (Fig. 7). It should be noted also that the correlation between H_2O and K_2O is notably poorer than those with La and Ce.

Compositions recalculated to 8 wt % MgO are shown in Fig. 8. Ridge-crest samples form a tight field indicating little variation in primitive magma compositions, consistent with conclusions of Batiza & Niu (1992). Off-axis samples generally display larger compositional variation. Glasses from each area have a narrower range of $Na_2O(8)$ values compared with Lamont Seamounts, but show a much larger range of $(La/Sm)_N(8)$, $H_2O(8)$, and $K_2O(8)$. This suggests that the contribution of variable F to the observed range of incompatible-element contents is minor compared with source heterogeneity. Unfortunately, a more quantitative analysis of the conditions of magma generation is hampered by the relatively evolved nature of the samples (mainly, unconstrained onset of clinopyroxene crystallization, which significantly affects the recalculated major-element contents at 8 wt % MgO), and unknown H_2O contents in the mantle source. A detailed mineralogical and petrological study needed to provide necessary constraints is beyond the scope of this paper.

Normalized trace-element contents in the ridge-crest glasses most closely resemble those of the high-La/Sm group of the Lamont Seamounts (Fig. 8a–c). The $^{87}Sr/^{86}Sr$ values of the ridge-crest glasses also plot within the field defined by Lamont Seamounts (Fig. 8d). The $^{87}Sr/^{86}Sr$ values of the off-axis lavas clearly correlate with $(La/Sm)_N(8)$ at $(La/Sm)_N(8) > \sim 0·8$ (Niu *et al.*, 1999; Regelous *et al.*, 1999; see also Fig. 8a and d), a typical feature of enriched northern EPR lavas in general (Zindler *et al.*, 1984; Niu & Batiza, 1997; Niu *et al.*, 1999; Regelous *et al.*, 1999; Castillo *et al.*, 2000).

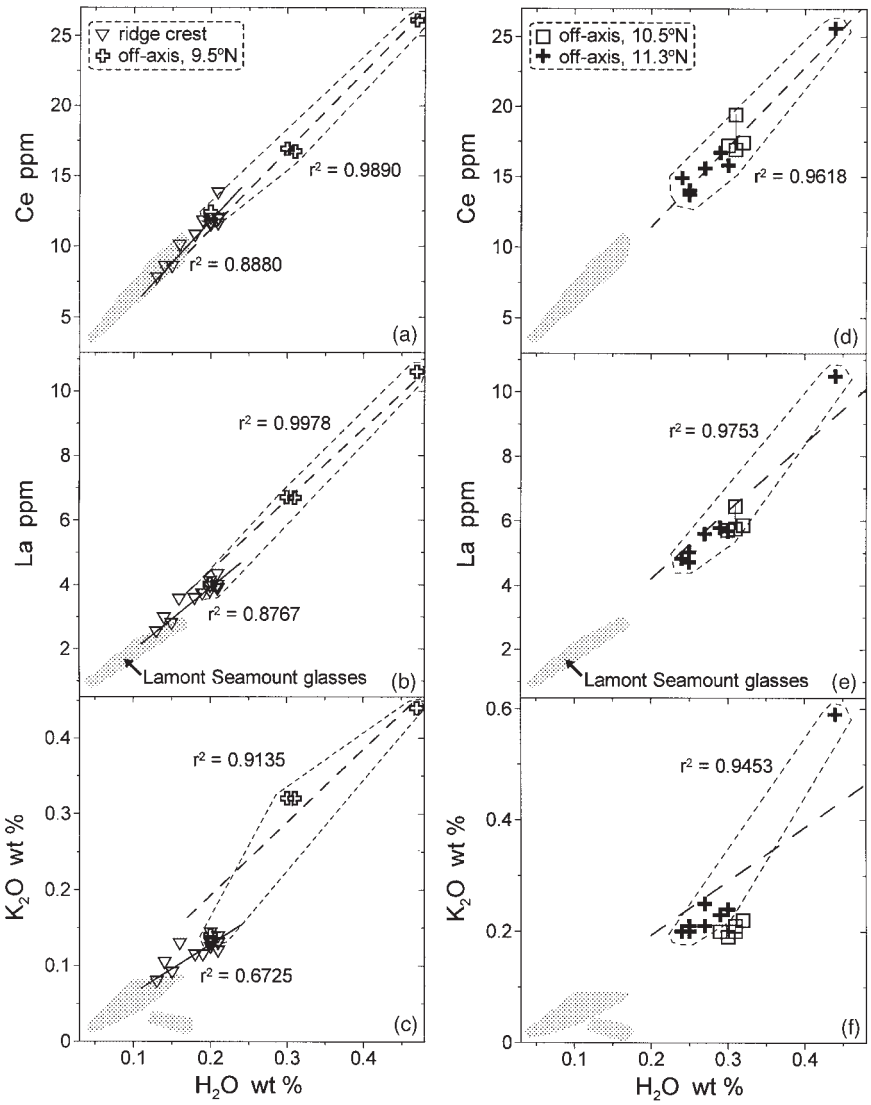

Fig. 7. H_2O contents of the normal-crust glasses between 9·3°N and 11·3°N. Continuous and dashed lines show least-squares linear best fits forced through the origin for the ridge-crest glasses and off-axis glasses from ~ 9·5°N and 11·3°N, respectively; correlation coefficients are for least-squares linear best fits not forced through the origin. The shaded fields for Lamont Seamount glasses are from Fig. 2.

Normal-crust samples with $(La/Sm)_N(8)$ within the range of Lamont Seamount glasses (ridge crest and off-axis at ~10·5°N) also have $H_2O/(Ce, La, or K_2O)(8)$ values similar to Lamont glasses (Fig. 9). At higher $(La/Sm)_N(8)$, $H_2O/La(8)$ progressively decreases (Fig. 9a), whereas H_2O/Ce remains roughly constant (Fig. 9b). H_2O/K_2O consistently decreases with increasing $(La/Sm)_N(8)$.

SEIR 127–129°E

Two segments, A1 (~127–127·5°E) and A2 (~127·5–129°E) of the SEIR immediately east from the Australian–Antarctic Discordance, were sampled extensively during cruise MW8801 of the R.V. *Moana Wave* in 1988 (Pyle *et al.*, 1992; Palmer *et al.*, 1993). A detailed petrological–geochemical study of the suite of dredged glasses and rocks has been given by Pyle (1994) and Pyle & Christie (in preparation). To summarize, samples cover a significant MgO range (8·5–4 wt %), although most dredge hauls have a narrow interval of MgO. Lavas vary in composition from incompatible-element depleted to non-depleted, with $(La/Sm)_N$ from 0·4 to 1. Most samples, however, have $(La/Sm)_N$ ~ 0·55, and these display major-element variations resembling those along an olivine + plagioclase + clinopyroxene cotectic (Pyle,

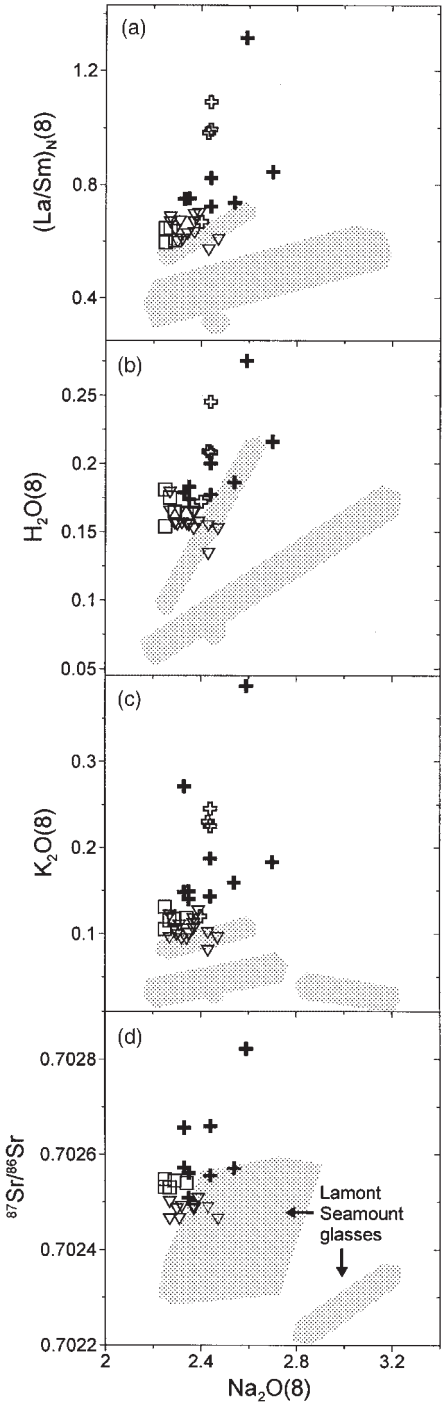

Fig. 8. Compositions of the normal-crust samples recalculated to 8 wt % MgO. Symbols as in Fig. 7. The fields for Lamont Seamount glasses are from Fig. 4. Normalization to primitive mantle of Sun & McDonough (1989). $^{87}Sr/^{86}Sr$ values are from Harpp *et al.* (1991), Niu *et al.* (1999), and Regelous *et al.* (1999).

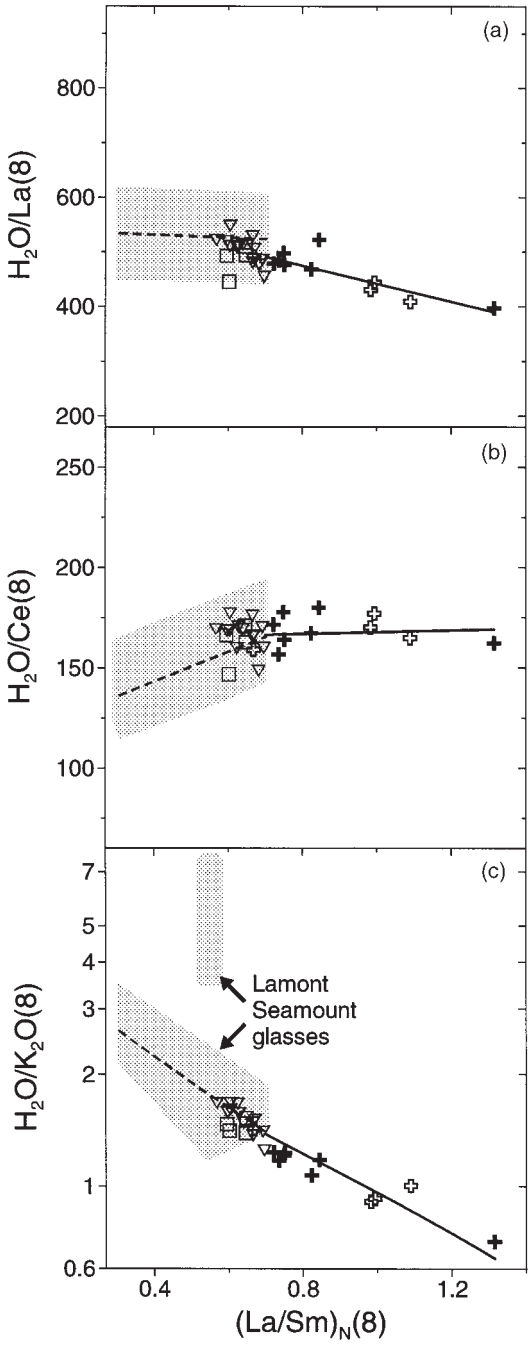

Fig. 9. Relative H_2O contents of the normal-crust samples. Symbols as in Fig. 7. The scale for each *y*-axis corresponds to that in Fig. 6 and is chosen so that the size of error bars is approximately similar for *y*- and *x*-axes in each plot. The field for Lamont Seamount glasses is from Fig. 6. Normalization to primitive mantle of Sun & McDonough (1989).

1994). All samples have a very limited range of depleted typical 'Pacific' Sr and Nd isotope ratios uncorrelated with $(La/Sm)_N$.

H_2O geochemistry

H_2O, major-, and trace-element contents in the SEIR glasses are presented in Tables 1 and 2. Variations in

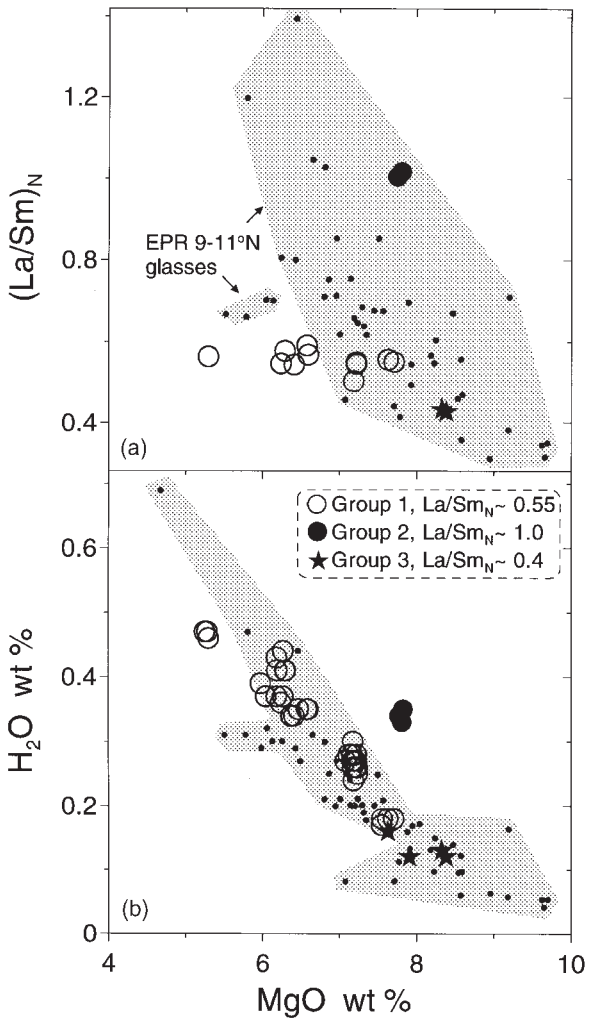

Fig. 10. $(La/Sm)_N$ (a) and H_2O (b) in glasses from SEIR at 127–129°E. The field of EPR 9–11°N glasses is shown for comparison. In (a), normalization to primitive mantle of Sun & McDonough (1989).

$(La/Sm)_N$ values at a given MgO allow them to be divided into three groups (Fig. 10a). Groups 2 and 3 cover a narrow MgO range at the most magnesian end of the spectrum. These are represented by samples from dredges 16 (segment A2) and 17 (segment A1), respectively, although glasses from Group 1 were found also in dredge 16. Group 2 glasses have the highest $(La/Sm)_N$ and H_2O contents at a given MgO, whereas Group 3 glasses have the lowest (Fig. 10b). The majority of the data (Group 1) covers a large range of MgO at a nearly constant $(La/Sm)_N$, and displays a correlation between H_2O and MgO (Fig. 10b).

Group 1 glasses also display a good correlation between H_2O and K_2O, La, or Ce (Fig. 11). As for the EPR glasses, the correlation between H_2O and K_2O is poorer. Group 3 glasses generally follow the Group 1 trend, although they appear to have slightly lower K_2O and La, whereas Group 2 glasses are significantly displaced from the Group 1 trend towards higher K_2O and La (Fig. 11b and c).

The role of fractionation in Group 1 glasses

To evaluate whether the major-element composition of the Group 1 glasses can be explained by fractionation alone, glass compositions were recalculated to 8 wt % MgO (Fig. 12; see Appendix B for calculation details). Glasses from segment A2 display a range of $Na_2O(8)$ contents similar to that of the Lamont Seamount glasses, whereas segment A1 glasses have a more restricted range of intermediate $Na_2O(8)$ values. Normalized glass compositions also have a range of $Al_2O_3(8)$ and FeO*(8) contents (Fig. 12b and c). This implies that Group 1 glasses were generated from a range of parental magma compositions.

Variations in compositions of Group 1 parental magmas

Although glasses from both segments appear to display a single trend of recalculated major oxides vs $Na_2O(8)$ (Fig. 12a–d), this trend is not consistent with parental magmas being produced either within a melting column or in an ascending diapir of a homogeneous major-element composition. The FeO*(8) vs $Na_2O(8)$ trend of Group 1 glasses (Fig. 12c) is even steeper than that of the Lamont Seamount glasses, excluding instantaneous melts from a melting column as parental magmas for Group 1 glasses (see Fig. 6). On the other hand, nearly constant $SiO_2(8)$ and CaO(8) in Group 1 magmas (Fig. 12a and d) are inconsistent with parental magmas being formed in a diapir (see Fig. 6) or representing accumulated melts of a melting column [see Niu & Batiza (1991, fig. 11)], as both these parameters should increase with decreasing $Na_2O(8)$ (increasing F) in both scenarios.

We conclude that major-element variations in Group 1 parental magmas do not reflect variable F of mantle sources with similar major-element contents, and thus should reflect source heterogeneity or some other process. The origin of these variations is not straightforward. For example, there is a negative correlation between $Na_2O(8)$ and incompatible-element contents for both segments (Fig. 13a–c), but it is different for each segment, i.e. segment A1 glasses have higher incompatible-element concentrations at a given $Na_2O(8)$. If variations in parental magmas are indeed related to major-element source heterogeneity, this implies that magmas from more fertile sources [higher $Na_2O(8)$] contain less incompatible

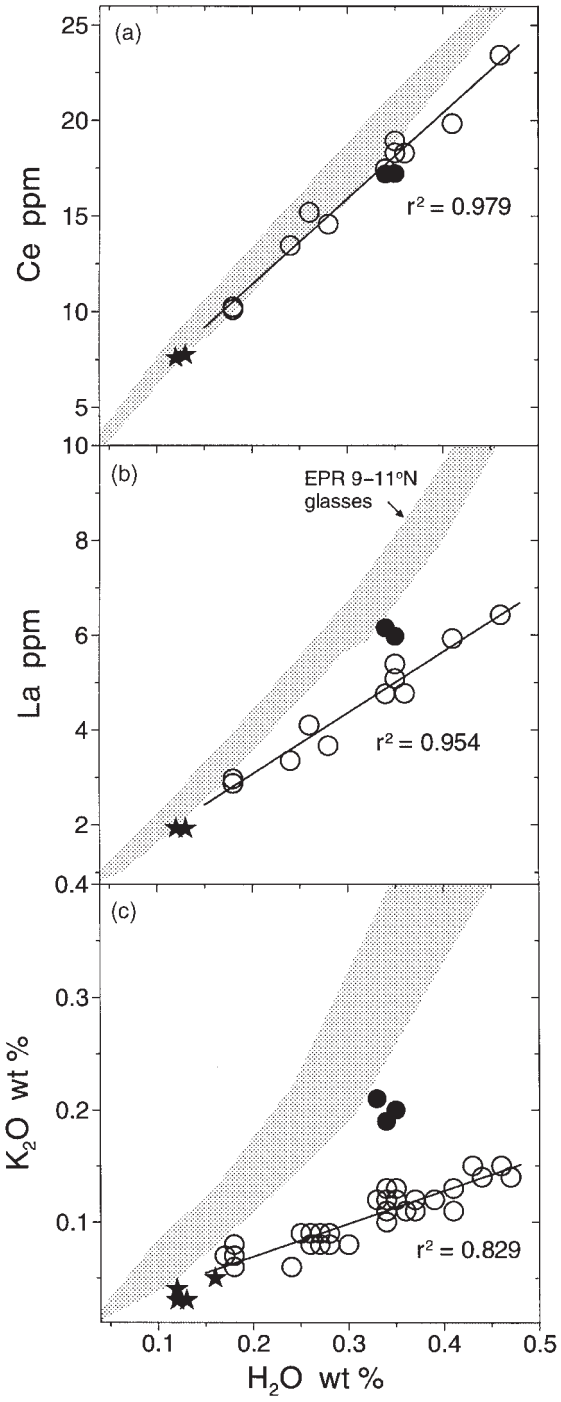

Fig. 11. H_2O contents in glasses from SEIR at 127–129°E. Symbols as in Fig. 10. Continuous lines show least-squares linear best fits for Group 1 glasses. The field of EPR 9–11°N glasses is shown for comparison.

elements. A detailed petrological study of this suite on these issues is beyond the scope of this study and will be presented by Pyle & Christie (in preparation).

Compositions of Group 2 and 3 parental magmas

Normalized major-element compositions of Group 3 glasses (low La/Sm) are in general similar to the composition of Group 1 glasses from segment A1 (Fig. 12a–d), indicating similar major-element characteristics of parental magmas. Thus, lower trace-element contents of Group 3 lavas (Fig. 13a–c) and their more depleted nature (lower La/Sm values, Fig. 12e) cannot reflect higher F of a source within the range of those for Group 1 from this segment [this would require lower $Na_2O(8)$ in Group 3 lavas, which is not observed]. As Sr, Pb and Nd isotopic compositions of Group 3 lavas are identical to those of Group 1 lavas [Pyle *et al.* (1992) and Fig. 12f], differences in trace-element contents cannot reflect long-lived mantle heterogeneities, as this would produce differences in radiogenic isotope ratios. A possible explanation is that these differences reflect melt redistribution during melting process, similar to the high- and low-La/Sm groups of Lamont Seamounts [see also Niu *et al.* (1996) for discussion on incompatible-element–isotope decoupling in the southern EPR].

Group 2 glasses (high La/Sm) have similar $Na_2O(8)$ and FeO*(8) to the Group 1 glasses from segment A2 recovered in the same dredge haul, but have significantly higher $Al_2O_3(8)$ and lower $SiO_2(8)$ and CaO(8). Such high $Al_2O_3(8)$ and low CaO(8) of Group 2 magmas resemble compositional features of very low F melts (see Fig. 6), but this is inconsistent with relatively low $Na_2O(8)$. The low CaO(8) and high $Al_2O_3(8)$ of Group 2 glasses may instead reflect early high-P clinopyroxene crystallization, but in any case it appears that high $(La/Sm)_N(8)$ and high incompatible-element contents of these glasses cannot be explained by lower F of the source of Group 1 lavas from the same part of segment A2. As Sr, Pb and Nd isotopic compositions of Group 2 lavas are also identical to those of Group 1 lavas [Pyle *et al.* (1992) and Fig. 12f], we again favour complexities in the melting process as the cause of trace-element differences between Group 2 and Group 1 magmas.

Relative H_2O contents

We have shown above that incompatible-element contents in Group 1 glasses from segments A1 and A2 are clearly different (Fig. 13a–c). However, incompatible-element ratio values in all glasses from both segments are the same. This can be seen in Fig. 13d–f for relative H_2O contents and in Fig. 12e for $(La/Sm)_N(8)$. In Fig. 13d–f, Group 1 glasses are spread equally along the least-squares linear best-fit lines that were forced through the origin. x/y values in x–y plots remain constant along such lines, and we see no systematic differences in relative H_2O contents of Group 1 glasses either between segments

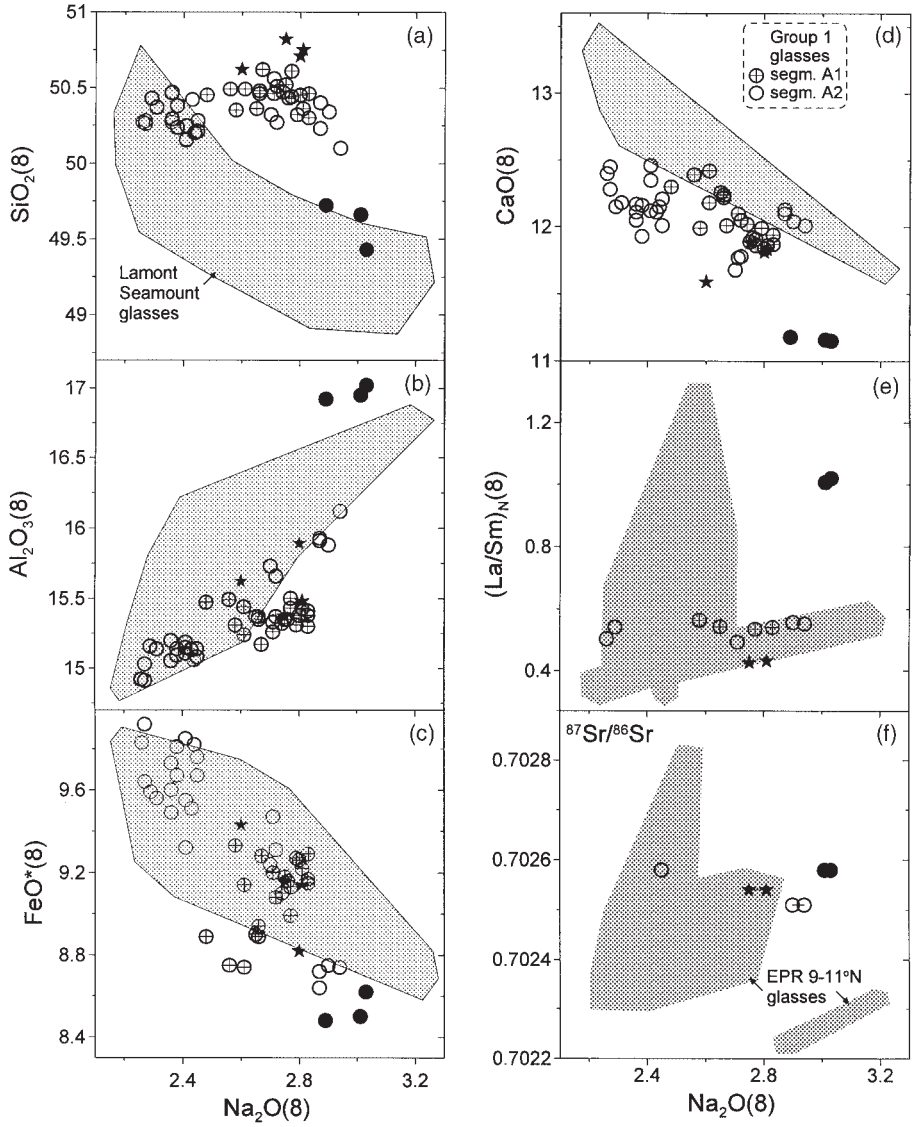

Fig. 12. Compositions of glasses from SEIR at 127–129°E recalculated to 8 wt % MgO. Group 1 glasses from segments A1 and A2 are shown separately. Other symbols as in Fig. 10. The fields of Lamont Seamounts glasses shown in (a)–(d) are from Fig. 4. The fields of EPR 9–11°N glasses shown in (e) and (f) are from Fig. 8. In (e), normalization to primitive mantle of Sun & McDonough (1989).

or at different $H_2O(8)$ values (Figs 13d–f and 14b–d). The scatter along the best-fit lines reflects analytical uncertainty and is similar to that observed in the EPR glasses (Fig. 13d–f). The average $H_2O/La(8) = 660 \pm 45$ (1σ), $H_2O/Ce(8) = 181 \pm 8$ (1σ), and $H_2O/K_2O(8) = 3{\cdot}0 \pm 0{\cdot}3$ (1σ).

Group 3 glasses have the same $H_2O/La(8)$ values as Group 1 (Figs 13e and 14b) but have higher $H_2O/K_2O(8)$ (displaced from the best-fit line towards higher H_2O) and lower $H_2O/Ce(8)$ (Figs 13d, f and 14b, c), whereas Group 2 glasses show an opposite pattern having lower $H_2O/K_2O(8)$ and higher $H_2O/Ce(8)$ than Group 1. As variations of relative H_2O contents within each group are mainly due to analytical uncertainties, we use averages for each group when comparing them with the EPR glasses.

SEIR glasses have higher $H_2O/(La, Ca, or K)(8)$ at a given $(La/Sm)_N(8)$ compared with the 9–11°N EPR glasses (Fig. 14b, c and d). Although SEIR glasses do not show the same continuous coverage of $(La/Sm)_N(8)$ as do EPR glasses, it appears that SEIR glasses are consistent with the patterns of covariations between

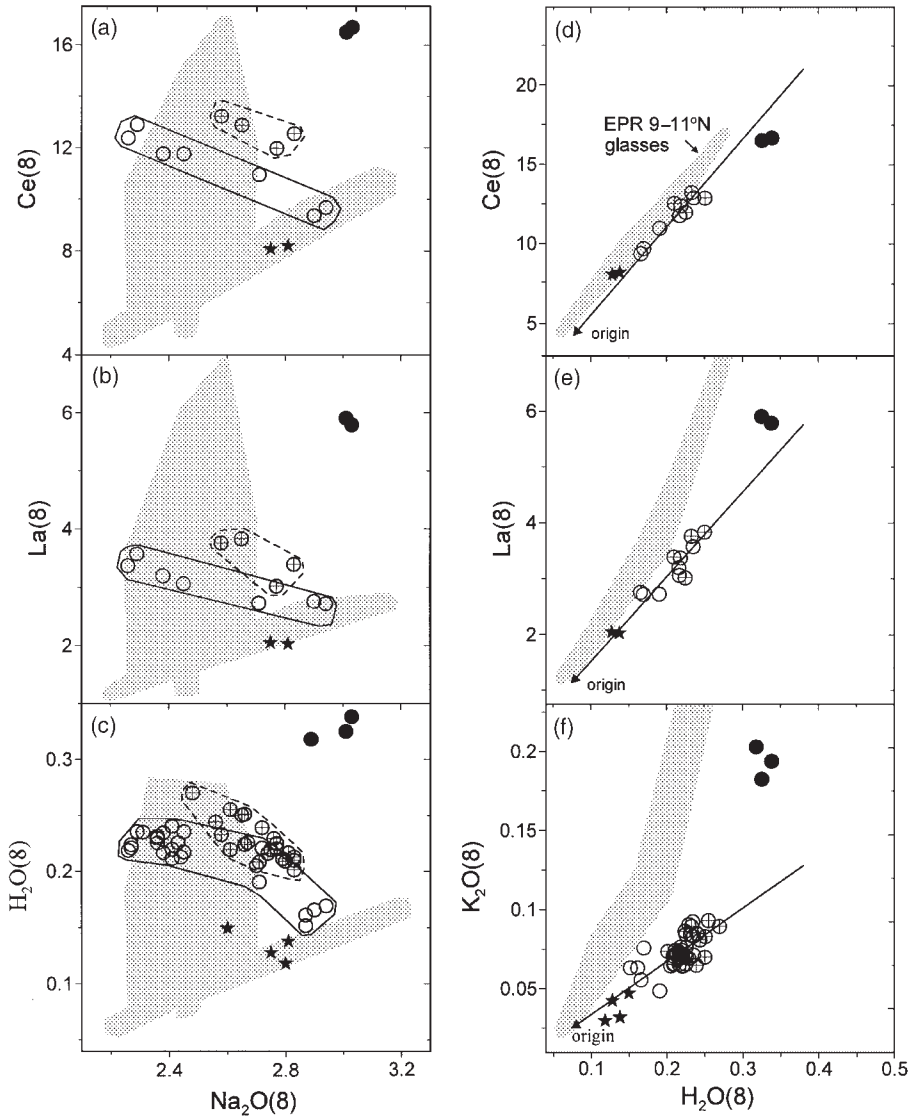

Fig. 13. Incompatible-element contents in glasses from SEIR at 127–129°E recalculated to 8 wt % MgO. Symbols as in Fig. 12. Continuous lines in (d)–(f) show least-squares linear best fits for Group 1 glasses forced through origin. The field of EPR 9–11°N glasses is shown for comparison.

relative H_2O contents and $(La/Sm)_N(8)$, as defined by the EPR glasses. As can be seen in Fig. 14, $H_2O/K_2O(8)$ decreases with increasing $(La/Sm)_N(8)$ in both suites, $H_2O/La(8)$ is nearly constant in glasses with $(La/Sm)_N(8) < \sim 0{\cdot}7$ and is lower at higher $(La/Sm)_N(8)$, whereas $H_2O/Ce(8)$ increases with increasing $(La/Sm)_N(8)$ in glasses with $(La/Sm)_N(8) < \sim 0{\cdot}7$ and is roughly constant at higher $(La/Sm)_N(8)$. These patterns of variations in relative H_2O contents with increasing $(La/Sm)_N(8)$ are discussed below.

DISCUSSION

The systematic pattern of variations in relative H_2O contents with increasing La/Sm

Degree of melting is not the main control of trace-element variability in studied MORB

Our analysis of chemistry of studied glasses has demonstrated that at least the following five factors shaped their compositions: (1) long-lived trace-element source

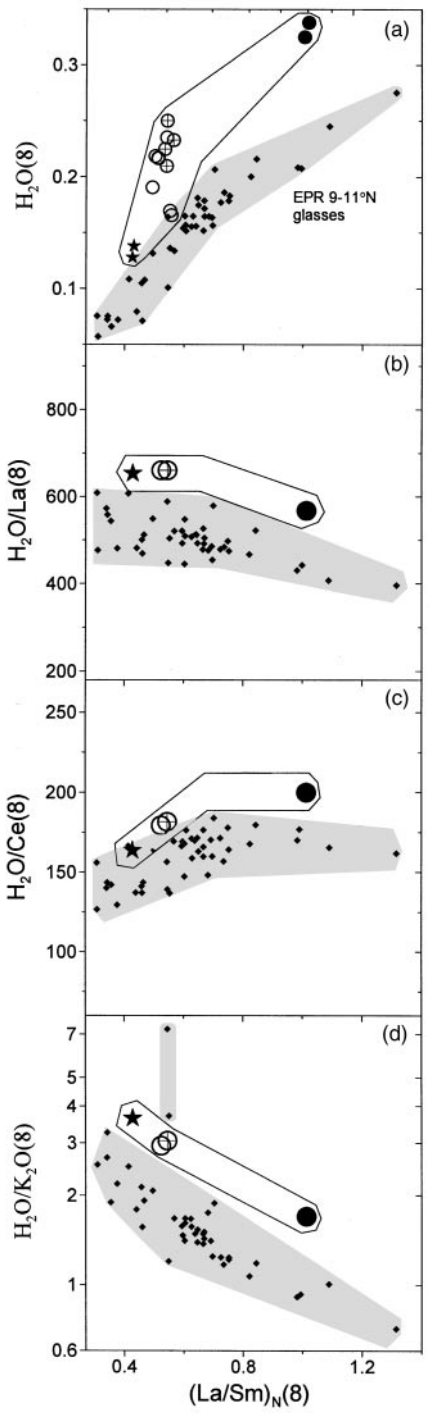

Fig. 14. $H_2O(8)$ and relative H_2O contents in glasses from SEIR at 127–129°E vs $(La/Sm)_N(8)$. Plots in (b)–(d) show average values for Groups 2 and 3 glasses and separate averages for segments A1 and A2 for Group 1 glasses. Data are shown as averages because variations of relative H_2O contents within each group mainly reflect analytical uncertainties. It should be noted that Group 1 glasses from segments A1 and A2 have virtually identical relative H_2O contents. Symbols as in Fig. 12. The fields of EPR 9–11°N glasses are from Fig. 9. Normalization to primitive mantle of Sun & McDonough (1989).

heterogeneity (normal crust EPR samples); (2) previous source depletion by separation of a small melt fraction (low-K group, Lamont Seamounts); (3) variations in source fertility (major-element heterogeneity) negatively correlated with trace-element abundances (Group 1, SEIR); (4) variations in the degree of melting (main and low-K groups, Lamont Seamounts); (5) some complex patterns of melt redistribution–migration within the melting region (high- and low-La/Sm groups, Lamont Seamounts; Groups 2 and 3, SEIR).

As can be inferred from our discussion of Lamont Seamount magma genesis (see above), the observed range of $Na_2O(8)$ in all studied glasses ($\sim$2·2–3·2 wt %, Fig. 12) implies that all of them were produced at total $F>5\%$ (assuming a reasonable range of source compositions), and none of them represents instantaneous melts from a melting column. This is important, as extreme variations in trace-element contents and ratios, which can be produced at very small F (e.g. Sobolev & Shimizu, 1993), cannot be invoked to explain the observed variability in our samples.

Because, in the case of the main and low-K groups of Lamont Seamount glasses, we demonstrated that the entire range of $Na_2O(8)$ present in our samples reflects variable F of a single source, this allows us to constrain the variations on $(La/Sm)_N$ that can be expected because of F over this range of $Na_2O(8)$. These variations, from 0·3 to 0·55 (Fig. 4e), are significantly less than the overall variations of $(La/Sm)_N$ observed in the studied suites (0·3–1·4 for the EPR glasses, 0·4–1 for the SEIR glasses), and therefore we consider F is not the major factor producing the observed variations in $(La/Sm)_N$, even when the isotopic composition of magmas with significantly different $(La/Sm)_N$ is similar (high- and low-La/Sm groups, Lamont Seamounts; Groups 2 and 3, SEIR).

H_2O behaviour is always similar to that of either La or Ce

Despite the number of very different processes and mechanisms involved in petrogenesis of studied samples, in all of them H_2O displays very strong correlations with the LREE and essentially mimics LREE geochemistry (Figs 2, 7, 8, 11, 13 and 14a). Moreover, in both studied regions, all glasses with $(La/Sm)_N < \sim 0{\cdot}7$ have constant values of $H_2O/La(8)$ within analytical uncertainty (530 $\pm$ 50 for EPR; 660 $\pm$ 45 for SEIR, Fig. 14b). This means that all five factors listed in the above section do not affect H_2O/La values, as all of them were identified in glasses with $(La/Sm)_N <0{\cdot}7$, and that in all of those processes H_2O behaves exactly as La. Thus, as expected (because La/Ce increases with increasing La/Sm, e.g. Fig. 5), H_2O/Ce increases with increasing $(La/Sm)_N$ in these glasses.

At the same time, all EPR glasses with $(La/Sm)_N$ >0·7 display constant $H_2O/Ce(8)$ (168 ± 8, Fig. 14c). This value is similar to the H_2O/Ce values in EPR glasses with $(La/Sm)_N$ of 0·6–0·7, and thus there is no discontinuity in the H_2O/Ce vs $(La/Sm)_N$ trend. As can be expected, H_2O/La decreases with increasing $(La/Sm)_N$ in these glasses. Although no glasses with $(La/Sm)_N$ of 0·7–1 are known from the studied area of the SEIR, samples with $(La/Sm)_N \sim 1$ from this region are consistent with the pattern shown by the EPR glasses. H_2O/La in the enriched SEIR samples is lower than in the depleted samples from this area, whereas H_2O/Ce is higher [note that the highest $(La/Sm)_N$ in the depleted group is 0·55, not 0·7]. Thus it appears that at $(La/Sm)_N > \sim 0{\cdot}7$, the geochemical behaviour of H_2O mimics that of Ce more closely than La.

Although glasses from both regions show the same patterns of variations in relative H_2O contents, there are clear regional differences in values of relative H_2O contents, which are higher in the SEIR glasses (Fig. 14). These regional differences will be discussed below.

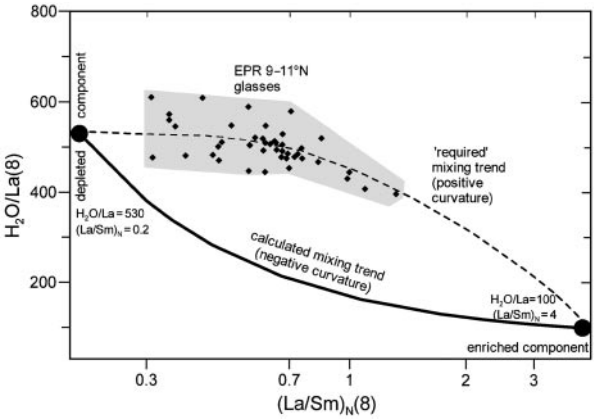

Fig. 15. Comparison of the observed $H_2O/La(8)$ vs $(La/Sm)_N(8)$ trend for 9–11°N EPR glasses from this study with the mixing trend between a depleted and an enriched component. H_2O/La in the depleted component (530) is equal to the average H_2O/La in Lamont Seamount glasses. H_2O/La for the enriched component (100) is slightly lower than the minimum H_2O/La value known in EMORB (Michael, 1995). (See text for discussion.)

Can the observed trends be explained by two-component mixing?

Well-known covariations of specific trace-element abundances and isotopic compositions of EPR lavas are consistent with the existence of long-lived heterogeneities in their mantle sources (e.g. Zindler *et al.*, 1984; Niu *et al.*, 1996; Castillo *et al.*, 2000). Recently, Niu & Batiza (1997) suggested that all observed trace-element variations in the northern EPR lavas can be explained by melting-induced two-component mixing. According to this hypothesis, the observed trends of relative H_2O contents vs $(La/Sm)_N$ represent parts of general mixing trends between a depleted component with $(La/Sm)_N$ <0·3 and an enriched component with $(La/Sm)_N$ >4. The enriched component has higher H_2O/Ce and lower H_2O/La values than the depleted component, and thus the observed constant values of H_2O/La at $(La/Sm)_N$ <0·7 and H_2O/Ce at $(La/Sm)_N$ >0·7 in our dataset are artefacts of limited sampling.

However, Figure 15 clearly demonstrates that the observed variations in H_2O/La cannot fit a mixing trend between any combination of the putative enriched and depleted components. This is because in x/y vs y/z plots, the curvature of a two-component mixing trend is fixed by the chosen ratio values of two endmembers and is independent of the absolute contents of x, y, and z. A positive curvature in such a plot, which is required to fit the data (Fig. 15), is possible only if H_2O/La in the enriched component is higher than in the depleted component. However, both our data and those from other regions (e.g. Michael, 1995) indicate that enriched glasses have lower H_2O/La than depleted glasses.

That a two-component mixing model cannot explain all incompatible-element variations in MORB glasses can also be seen in the dataset of Niu & Batiza (1997). For example, Fig. 16 shows several ratio/ratio plots with a common denominator. In x/y vs z/y plot, two-component mixing generates a straight line. However, none of the actual data form a single straight line.

The above discussion does not imply that the source of most MORB is homogeneous, or that melting-induced mixing is not an important process during MORB magma genesis; however, it does show that two-component mixing cannot explain the observed shapes of the variation trends for all incompatible-element ratios vs La/Sm.

Possible explanations for the observed variations in H_2O/La and H_2O/Ce with increasing La/Sm

Differences in magma generation processes beneath the ridge and under seamounts

In general, our data for the 9–11°N EPR glasses can be interpreted as follows: $H_2O/La(8)$ is constant for the seamounts, but for all normal-crust samples, it decreases with increasing $(La/Sm)_N(8)$, whereas $H_2O/Ce(8)$ remains constant (Fig. 9). This interpretation implies that H_2O geochemistry is controlled by different factors during magma genesis of Lamont Seamount and normal-crust lavas; i.e. H_2O is similar to La in the former, but it is similar to Ce in the latter. Although this interpretation may be appealing, as different magma generation processes beneath the ridge and under seamounts might be expected (e.g. Lundstrom *et al.*, 1999), we do not favour

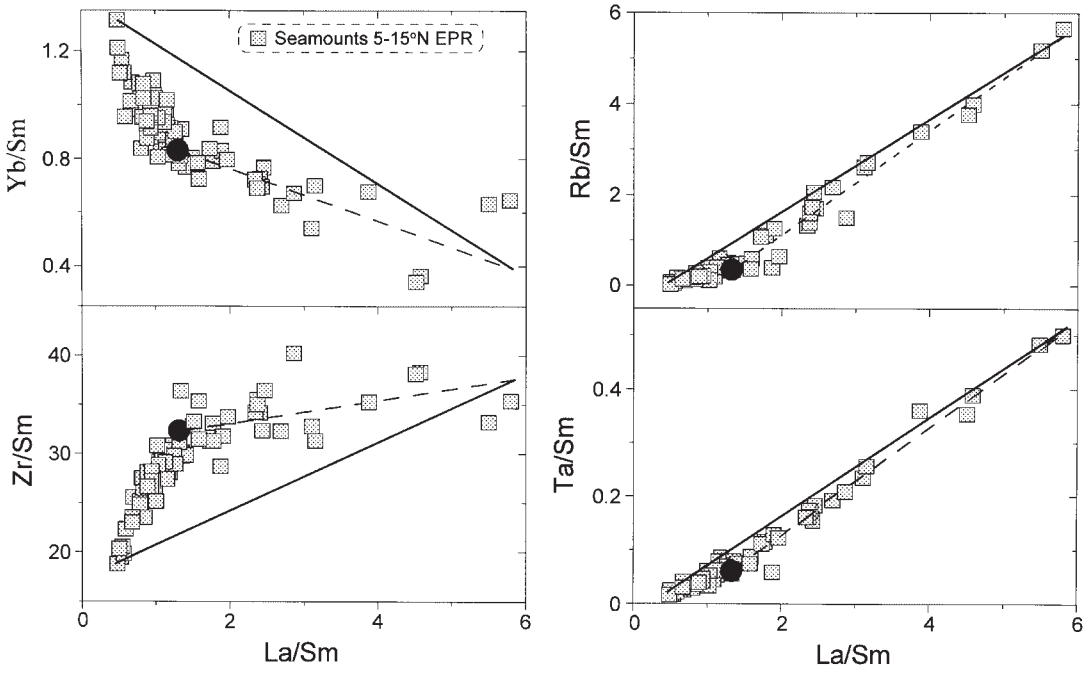

Fig. 16. *x/y* vs *z/y* plots with the dataset of Niu & Batiza (1997) of the near-EPR seamount glasses between 5 and 15°N. Mixing trends in such diagrams are always a straight line (continuous lines show mixing trends between the most enriched and most depleted composition). It is clear from this plot that the entire range of trace-element variations in these glasses cannot be explained by a two-component mixing as the data fit curved trends. However, glasses with La/Sm >1·32 [$(La/Sm)_N$ >0·85] conform to a straight line and thus can be explained by a two-component mixing. Dashed lines show linear best fits through data with La/Sm >1·32. ●, compositions along the best-fit lines at La/Sm = 1·32. (See text for discussion.)

this explanation because $H_2O/La(8)$ is also constant in the ridge-crest 127–129°E SEIR magmas with $(La/Sm)_N(8)$ <0·7 (Figs 13e and 14b). Although samples with $(La/Sm)_N(8)$ between 0·6 and 1 are not known from this part of the SEIR, the most enriched glasses from this area have lower $H_2O/La(8)$ than the depleted glasses, suggesting a similar style of variation in relative H_2O contents in different regions and in normal-crust samples.

A combination of melting and mixing controls

For glasses with $(La/Sm)_N < \sim 0{\cdot}7$, we identified three melting-related processes (i.e. previous source depletion by separation of a small melt fraction; variations in the degree of melting; melt redistribution–migration within the melting region) to be the cause of trace-element ratio variations. In contrast, trace-element source heterogeneity is the main factor controlling trace-element variations in the 9–11°N EPR glasses with $(La/Sm)_N$ >0·7 (Fig. 8a). Thus, one can suggest that during melting, H_2O always behaves like La, i.e. H_2O incompatibility equals that of La during MORB magma genesis [see a detailed discussion on determining element incompatibilities given by Sims & DePaolo (1997)]. However, mixing processes (dominating at $(La/Sm)_N > \sim 0{\cdot}7$) obscure this relationship, as the enriched component has lower H_2O/La values than the source of NMORB.

H_2O is not the only incompatible element for which ratios to REE of similar incompatibility in northern EPR magmas change with increasing La/Sm in this fashion. Figure 17 shows ratios of P, Zr and Hf to middle REE (MREE) for near-EPR seamounts between 5 and 15°N (Niu & Batiza, 1997). P/Dy values remain constant in the depleted glasses whereas P/Sm and P/Nd values increase with decreasing La/Sm. On the other hand, P/Nd values remain constant in the enriched glasses, whereas P/Sm and P/Dy increase. This results in a V-shaped pattern in the P/Sm vs La/Sm plot. Zr changes from Pr-like in the depleted glasses to Sm-like in the enriched glasses, with Zr/Nd showing a V-shaped pattern (similar to P/Sm). Hf is similar to Sm in the enriched glasses and is intermediate between Nd and Sm in the depleted glasses. In the enriched glasses, Zr and Hf change towards more compatible REE, similar to H_2O, whereas P changes in the opposite direction. We also note that samples from the SEIR are consistent with the pattern defined by the northern EPR magmas (Fig. 17), although they obviously cannot be used to confirm the EPR pattern because of a limited range of $(La/Sm)_N$.

On the basis of the V-shaped patterns in the P/Sm, Zr/Nd, and Hf/Sm plots (Fig. 17), a change in relative incompatibility occurs for each element at $(La/Sm)_N$ $\sim 0{\cdot}85$. Although we inferred that H_2O changes from

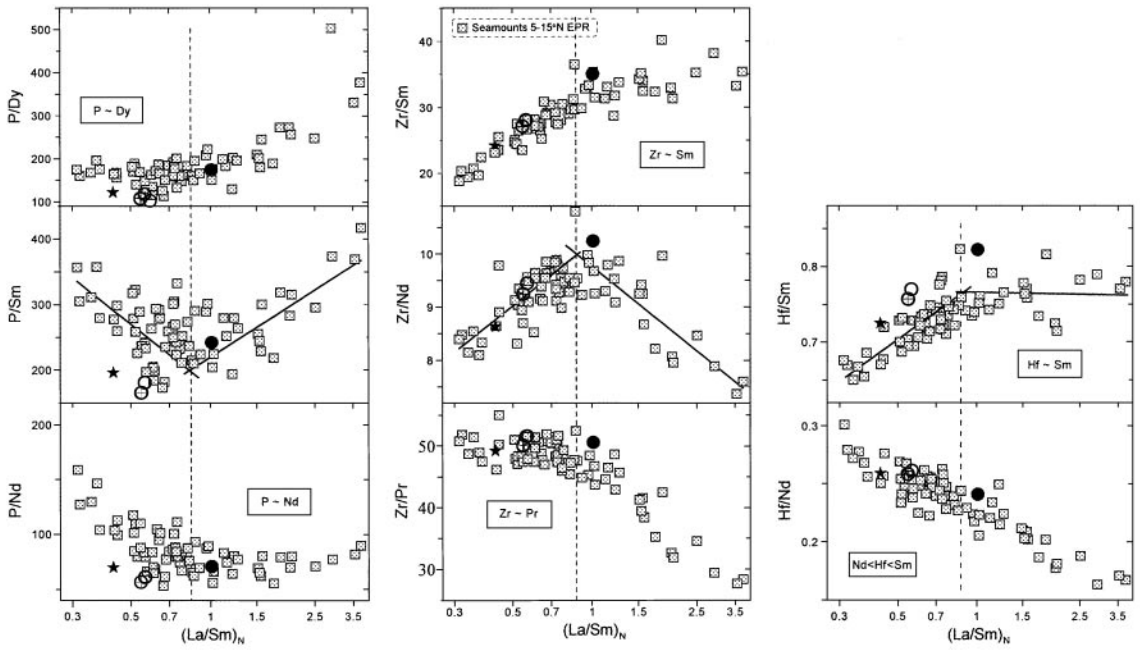

Fig. 17. Variations in P, Zr, and Hf contents relative to the middle REE in 5–15°N EPR near-ridge seamount glasses (Niu & Batiza, 1997) and SEIR glasses (this study). SEIR data are represented by averages of Groups 1 (separately for segments A1 and A2), 2, and 3. Symbols as in Fig. 14. Continuous lines in P/Sm, Zr/Nd, and Hf/Sm plots are least-squares best fits through seamount data with $(La/Sm)_N$ <0·7 and $(La/Sm)_N$ >1. Vertical dashed lines in each set of plots show the position of the intersection of best fits through depleted and enriched glasses. It should be noted that in all three plots, these lines are at a similar position of $(La/Sm)_N \sim 0{\cdot}85$. (See text for discussion.) Normalization to primitive mantle of Sun & McDonough (1989).

La-like to Ce-like at $(La/Sm)_N \sim 0{\cdot}7$, it is clear from Fig. 14 that our data are also consistent with a value of 0·85 (because of a limited number of enriched glasses in our dataset).

Assuming that $(La/Sm)_N \sim 0{\cdot}85$ marks the change in ratios of H_2O, P, Zr, and Hf to REE of similar incompatibility, we can then rephrase our working hypothesis as: H_2O incompatibility equals that of La during MORB magma genesis [and P ~ Dy, Zr ~ Pr, Hf ~ (Sm + Nd)/2], but mixing processes, dominating at $(La/Sm)_N$ >0·85, obscure this relationship, as the enriched component has lower H_2O/La, Zr/Pr, and Hf/[(Sm + Nd)/2], and higher P/Dy than the source of NMORB.

The idea that mixing dominates the trace-element signature in MORB magmas at $(La/Sm)_N$ >0·85 only, whereas its contribution is minor in more depleted compositions where melting processes are dominant in determining the trace-element composition, is also consistent with element ratios plotted in Fig. 16, as all of them can be approximated by a straight line at $(La/Sm)_N$ >0·85 (La/Sm >1·32).

However, there are also some problems with this model. First, the most enriched glasses from the SEIR do not show evidence for trace-element source heterogeneity, but nevertheless have lower H_2O/La than NMORB samples from this area (Fig. 14b). This is a serious problem, as our working hypothesis implies that H_2O/La in MORB can be changed only as a result of mixing of components with initially different H_2O/La values. Second, it is not clear why the enriched component has similar values of H_2O/Ce, P/Nd, Zr/Sm, Hf/Sm (and possibly some other element ratios) to the least depleted NMORB, given an ultimate origin of the enriched component as recycled oceanic crust (e.g. Hofmann, 1988; Saunders *et al.*, 1988; Mahoney *et al.*, 1994; Niu & Batiza, 1997). Third, the model cannot explain regional differences in H_2O/La between NMORB [see detailed discussion of the last two issues by Michael (1995)].

Changes in the relative incompatibility of H_2O with increasing $(La/Sm)_N$

Yet another possibility is that a change in incompatibility relative to REE (relative incompatibility) with increasing La/Sm for a number of elements is a general feature of MORB magma genesis. According to this model, during genesis of magmas with $(La/Sm)_N$ >0·85, H_2O incompatibility equals that of Ce, P ~ Nd, and Zr ~ Hf ~ Sm. This model implies that H_2O/Ce, P/Nd, Zr/Sm, and Hf/Sm values in the enriched lavas reflect these values in their sources and are not affected by melting, whereas in the more depleted magmas [$(La/Sm)_N$ <0·85],

these ratios are affected by melting but H_2O/La, P/Dy, Zr/Pr, and Hf/[(Sm + Nd)/2] values remain constant and reflect the values of their sources.

Trace-element source heterogeneity sampled by E-MORB may be accommodated either by variably enriched peridotites (e.g. Niu *et al.*, 1996) or by lithologically heterogeneous mantle [i.e. peridotites and pyroxenites in a 'marble-cake mantle' (Allègre & Turcotte, 1986), or peridotites and garnet pyroxenites (Hirschmann & Stolper, 1996)], where pyroxenites represent remnants of subducted material (i.e. the recycled component). The incompatible-element-enriched signature of EMORB magmas produced by melting-induced mixing of heterogeneous mantle (e.g. Prinzhofer *et al.*, 1989; Hirschmann & Stolper, 1996) is expected to be dominated by melts produced from the recycled component (enriched domains). As incompatible elements and H_2O probably reside in clinopyroxene in the source (see discussion below on H_2O storage in the mantle), incompatible-element ratios (including relative H_2O contents) in MORB magmas should depend on clinopyroxene/melt K_d values in depleted and enriched sources. If we assume that clinopyroxene compositions are different in depleted and enriched sources, it is realistic to expect slightly different relative incompatibilities of elements within the REE range of incompatibility (Blundy *et al.*, 1996; Wood & Blundy, 1997).

This also explains why a similar change cannot be observed when elements with very different incompatibilities are compared. For example, Rb (and also Ba, Cs, Nb, Ta, Th, U, K) is always more incompatible than any REE, and thus Rb/REE values increase with increasing (La/Sm) over the entire range from extremely depleted to extremely enriched compositions. REE are a useful denominator in element ratios for this type of analysis because their order of incompatibility remains the same across the entire MORB compositional spectrum.

We also emphasize here that the major-element composition of EMORB is probably dominated by peridotite-source melts. This is because primitive EMORB have very magnesian liquidus olivines (up to $Fo_{91·3}$), which are sometimes even more primitive than those in surrounding NMORB (e.g. Sobolev *et al.*, 1989; Dmitriev *et al.*, 1991), indicating very high *mg*-number of EMORB parental magmas. This cannot be achieved during melting of pyroxenites. However, this conclusion does not contradict the above explanation of trace-element variability, as additions of small amounts of enriched melts to peridotite-derived NMORB magmas will significantly affect incompatible-element contents with little impact on major elements.

An explanation for the lower H_2O/La values in the most enriched SEIR lavas requires a mechanism that would allow, first, impregnation of the NMORB-like source of these lavas with a small-*F* melt from a similar source. Although this enriches the source in highly incompatible elements, H_2O/La in this enriched source should be the same as in NMORB from this area. However, if the enriched (small-*F*) melt freezes, this will change the composition of clinopyroxene in the source, and H_2O becomes more compatible than La in this new source composition. Remelting of this new source to a relatively small *F* [supported by high Na_2O(8) of these lavas, Fig. 12] can then produce magmas with lower H_2O/La. However, the virtually identical Sr, Nd, and Pb isotopic compositions of EMORB and NMORB from this area require that all these events happen within a limited time interval. That such a mechanism can occur is supported by the presence of the enriched SEIR lavas exclusively at the very tip of the propagating spreading centre (Palmer *et al.*, 1993). Thus new upwelling associated with the propagator can reactivate frozen peripheral parts of the melting region of the dying spreading centre.

Although this model can better explain the constant H_2O/Ce (and other element ratios) in enriched MORB, and reconciles similar shapes of trends in plots of relative H_2O contents vs $(La/Sm)_N$ in two regions, it also has problems. Similar to the previous model, it is not clear why the enriched component has similar values of H_2O/Ce (and P/Nd, Zr/Sm, Hf/Sm) to the least depleted NMORB from this area. It is also unclear whether the change in relative incompatibility of H_2O (and also P, Zr, Hf) at $(La/Sm)_N \sim 0·85$ is a general feature of MORB, or whether this value is different for different regions and is determined by the composition of the enriched component [note that we cannot constrain the $(La/Sm)_N$ value at which this change occurs in the SEIR lavas]. Also similar to the previous model, this model cannot explain regional differences in H_2O/La between NMORB.

Despite these problems, at the moment we favour changes in relative incompatibility as the cause of observed variation in relative contents of H_2O, P, Zr, and Hf. An important implication of this phenomenon is that an artificial depletion (or enrichment) of these elements relative to REE will appear when depleted and enriched lavas are plotted together on normalization diagrams using any particular order of incompatibility. The same phenomenon probably occurs for more incompatible elements, outside the REE range of incompatibility; however, these are more difficult to constrain, as discussed above, and that task is outside the scope of this paper.

Regional differences in relative H_2O contents

Our results demonstrate that although magmas from the EPR and SEIR display similar patterns of covariation between relative H_2O contents and $(La/Sm)_N$, relative

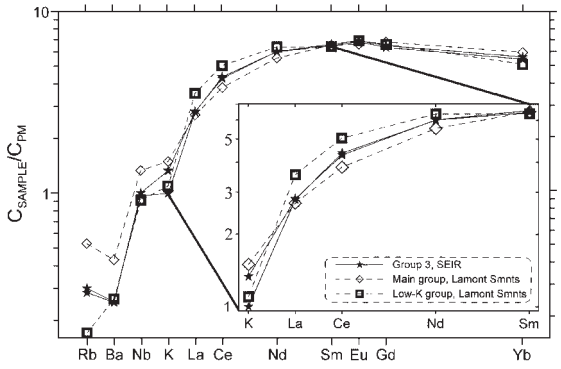

Fig. 18. Primitive mantle-normalized incompatible-element contents of Group 3 SEIR glasses compared with a main group Lamont Seamount glass with similar La/Sm. This figure demonstrates that Group 3 SEIR glasses are more depleted in strongly incompatible elements and less depleted in Ce and Nd than Lamont Seamount glasses. This results in lower La/Ce in the SEIR glasses at a given $(La/Sm)_N$. A low-K group Lamont Seamount glass is shown for comparison. The insert enlarges a part of the spectra from K to Sm. (See text for discussion.) Normalization to primitive mantle of Sun & McDonough (1989).

H_2O contents are generally higher in the SEIR glasses (Fig. 14). Regional variations in relative H_2O contents on a global scale have been demonstrated previously by Michael (1995). In our samples, $H_2O(8)$ values are also higher in the SEIR glasses for a given $(La/Sm)_N$, and this difference increases at higher $(La/Sm)_N$ (Fig. 14a).

The importance of melting-induced mixing between the NMORB source and remnants of the recycled crust material (e.g. Hofmann, 1988; Saunders *et al.*, 1988; Prinzhofer *et al.*, 1989; Mahoney *et al.*, 1994; Niu *et al.*, 1996; Hirschmann & Stolper, 1996; Niu & Batiza, 1997) in the magma genesis of EMORB can explain regional variations in their relative H_2O contents. These variations can simply reflect variations in the composition of the recycled component (note, however, that higher relative H_2O contents in the most enriched SEIR samples, compared with the EPR, have a different origin and are caused by higher relative H_2O contents in the depleted samples from this area; see above). In general, enriched magmas with higher relative H_2O contents can originate from a source that was formed by addition to the NMORB source of a recycled material that had lost relatively less H_2O during subduction [i.e. cooler subduction zones (Schmidt & Poli, 1998)]. As discussed above, H_2O and the LREE appear to be coupled in all processes of source evolution, and it may follow that during subduction to deeper levels in the mantle, H_2O, which is left in the slab after dehydration, and the LREE are stored together in pyroxene during all recycling processes. This would explain why the original variations in H_2O/LREE values are preserved and transported via convection in the mantle to the areas of present-day MORB magma genesis.

However, as discussed in detail by Michael (1995), such mixing cannot explain the observed differences in relative H_2O contents between NMORB from different areas, as it cannot affect significantly the compositions of depleted lavas. We hypothesize that regionally different H_2O/La values in NMORB must reflect either initial variations of this ratio in the Earth's mantle or inhomogeneities left after formation of the continental crust. However, more complex and quantitative explanations are under development (Danyushevsky, in preparation).

An important consequence of our study is that regional differences can be defined only by suites that display a large range of $(La/Sm)_N$ values over which there are systematic differences in relative H_2O contents (e.g. EPR vs SEIR). For example, if our collection was limited to the depleted SEIR lavas and enriched EPR lavas only (or vice versa), regional differences would not be apparent (Fig. 14), leading to very different conclusions about H_2O geochemistry.

Why are H_2O/Ce values in the most depleted SEIR glasses within the range of EPR glasses?

As can be seen in Fig. 14, all relative H_2O contents in the SEIR glasses are higher than in the EPR glasses, except for H_2O/Ce in Group 3. Figure 18 compares normalized incompatible-element spectra of the Group 3 glasses with glass 1562-2112 from the main group of Lamont Seamounts, which has similar $(La/Sm)_N$ (0·43 and 0·41, respectively). Group 3 glasses are more depleted in strongly incompatible elements, but are less depleted in Ce and Nd than the main group Lamont samples. This is reflected in lower La/Ce of the Group 3 glasses at a given $(La/Sm)_N$, and thus Group 3 glasses would have lower H_2O/Ce values at similar H_2O/La. These features of the Group 3 samples mimic those of the low-K group of the Lamont Seamounts (Fig. 18). However, in the case of the SEIR suite, this is a general feature, as Group 1 glasses from this area also have lower La/Ce compared with Lamont glasses at a given $(La/Sm)_N$ (Fig. 5a). This indicates that the mantle source of the SEIR samples is regionally more depleted in highly incompatible elements than the source of Lamont Seamount magmas.

We also note that regional differences in relative H_2O contents do not necessarily indicate differences in absolute H_2O contents in mantle sources, as higher relative H_2O contents may reflect lower REE contents.

H_2O storage in the mantle

An important result of this paper is that in all studied samples, regardless of the origin and previous history of

their mantle sources, H_2O displays very strong correlations with the LREE and essentially mimics their geochemistry (Figs 2, 7, 8, 11, 13 and 14a). As discussed above, this suggests that the same factors affect the geochemistry of the LREE and H_2O in all processes leading to the final composition of the erupted magmas. We believe that this puts constraints on the H_2O storage and transport in the MORB source, and necessarily implies that H_2O resides in the same phases as the LREE in all sources during all processes. In the region of partial melting, this phase is obviously a silicate melt. However, if the deep mantle is under subsolidus conditions (e.g. Green & Falloon, 1998), H_2O then must be stored in the same mineral(s) as the LREE.

If we assume that the studied samples are representative of MORB in general, our results argue for the absence of a free H-bearing fluid phase in the deep mantle (in the form of H_2O, CH_4, or H_2). If such a fluid was initially present and then incorporated into the melt, contributing the bulk of H_2O (e.g. Green *et al.*, 1987), it would be difficult to explain excellent correlations between H_2O and LREE observed in all studied glasses. We consider this unlikely, as it requires that the exact amount of fluid needed to produce such correlations was added to each melt despite demonstrated differences in source compositions and F, and also possible melt redistribution processes during magma genesis.

Another strong argument in support of H_2O residing in a major silicate mineral in the mantle is that the H_2O/La values in NMORB are not affected by the removal of a small melt fraction, as clearly demonstrated by anomalously depleted samples from the Lamont Seamounts. These samples were probably formed from a source that has previously lost most elements more incompatible than La. We suggest that this depletion involved separation of a small melt fraction, as it affected high field strength elements, LREE and large-ion lithophile elements (e.g. Nb, Rb, Ba, K, La, Figs 3 and 6a). If H_2O resided in some exotic minerals or in a fluid phase in subsolidus conditions, it would have been lost during this earlier melting event, resulting in low relative H_2O contents of the anomalously depleted Lamont Seamount lavas, which is not observed. The absence of exotic minerals in the MORB source is also supported by the fact that peridotite trace-element contents can be successfully modelled by combining trace-element contents of major rock-forming minerals in their modal proportions (Eggins *et al.*, 1998*b*). We also note here that generally poorer correlations between H_2O and K_2O compared with H_2O and the LREE (Figs 2, 7 and 11) may reflect generally variable degrees of depletion of the MORB source during its previous history. In cases of extreme depletion, as for samples discussed above, this causes anomalously high H_2O/K_2O values, but in less extreme situations it can cause the observed 'noise' in the H_2O–K_2O correlations.

Our results argue against olivine control over H_2O geochemistry (e.g. Hirth & Kohlstedt, 1996). As clinopyroxene is considered to be the main host of the LREE in the solid mantle (e.g. Johnson *et al.*, 1990; Wood & Blundy, 1997), this mineral must also contain the bulk of mantle H_2O. If this were not the case, different minerals would determine the bulk K_d of H_2O and LREE during melting, which should result in changes of relative H_2O contents with increasing F. This is not observed (constant H_2O/La in the main and low-K groups of Lamont Seamount glasses). Our conclusions are also indirectly supported by the experimental data of Kohn (1996), who demonstrated higher solubility of H_2O in clinopyroxene relative to olivine and orthopyroxene.

Reconciling previous studies of H_2O geochemistry in MORB

Our results indicate that conclusions on H_2O incompatibility depend on the range of $(La/Sm)_N$ of the dataset used. The dataset of Dixon *et al.* (1988) from Juan de Fuca Ridge was dominated by glasses with $(La/Sm)_N$ <0·85, and thus that study concluded that H_2O behaves like La. The dataset of Michael (1995) and their data treatment were dominated by EMORB samples, and thus Michael (1995) concluded that H_2O behaves like Ce.

The conclusion of Jambon & Zimmermann (1990) that H_2O incompatibility equals that of K_2O resulted from an incomplete dataset and over-generalization (a summary of their ideas is given in the Introduction). Indeed, glasses with H_2O/K_2O >4 are very rare (but known from ODP Hole 896a; McNeill & Danyushevsky, 1996; Danyushevsky *et al.*, in preparation) because such high values can be found in strongly depleted glasses only (Fig. 14d), and the number of such samples is very limited. However, when a suite of NMORB is studied in detail, it is clear that H_2O is more compatible than K_2O, similar to La.

CONCLUSIONS

This paper demonstrates that values of H_2O/(La, Ce, or K_2O), i.e. relative H_2O contents, vary systematically with increasing $(La/Sm)_N$ in MORB glasses from both the EPR and SEIR. This indicates that H_2O behaves like any other incompatible trace element during MORB petrogenesis, and therefore does not require any special processes (e.g. fluid contribution) in addition to those required to explain the incompatible-element geochemistry of MORB. The relative H_2O contents of MORB glasses from the SEIR and EPR are distinct,

demonstrating significant regional variations in the H_2O geochemistry of MORB.

The incompatible behaviour of H_2O is similar in both studied regions. H_2O relative incompatibility varies systematically with increasing $(La/Sm)_N$: in depleted MORB H_2O is similar to La, whereas in EMORB H_2O is similar to Ce, and H_2O is more compatible than K_2O at all values of $(La/Sm)_N$. We also suggest that H_2O is not the only element for which incompatibility (relative to REE) is different in NMORB and EMORB. Similar patterns of varying relative incompatibility are displayed by Zr, Hf, and P.

Our data are best explained if H_2O is stored in the same phase with LREE (probably clinopyroxene) below the mantle solidus. Regional variations in relative H_2O contents in EMORB that have more radiogenic Sr, Nd and Pb isotopes than NMORB can be explained by differences in the nature of enriched components recycled via subduction processes. However, when EMORB has the same radiogenic isotope compositions as NMORB within a region, relative H_2O contents in EMORB are probably controlled by the relative H_2O contents of nearby NMORB.

Regional differences in relative H_2O contents of NMORB probably reflect either initial variations of this ratio in the Earth's mantle or inhomogeneities left after formation of the continental crust.

ACKNOWLEDGEMENTS

L.V.D. offers special thanks to Rodey Batiza for donating samples of the EPR glasses and for numerous discussions on MORB geochemistry. Stimulating discussions with Peter Michael, Doug Pyle, Tony Crawford, and Jon Snow over the last 3 years have significantly improved the manuscript. We would like to thank especially Tony Crawford for patiently reading numerous earlier versions of this paper. Dima Kamenetsky provided useful critical comments on an earlier version of the manuscript and helped with LA-ICP-MS analyses. This research was supported by the Australian Research Council. We acknowledge support of the Museum of Natural History, Washington, DC, which provided electron microprobe standards. Editorial comments by Richard Arculus and an anonymous reviewer have improved this paper. We also acknowledge the critical reviews of Jacqueline Dixon, Yaoling Niu, and an anonymous reviewer during the 2·5 years that this paper was under consideration for publication by the editors of the *Journal of Geophysical Research*.

REFERENCES

Aggrey, K. E., Muenow, D. W. & Batiza, R. (1988). Volatile abundances in basaltic glasses from seamounts flanking the East Pacific Rise at 21N and 12–14N. *Geochimica et Cosmochimica Acta* **52**, 2115–2119.

Allan, J. F., Batiza, R, Perfit, M. R., Fornari, D. J. & Sack, R. O. (1989). Petrology of lavas from the Lamont seamount chain and adjacent East Pacific Rise, 10°N. *Journal of Petrology* **30**, 1245–1298.

Allègre, C. J. & Turcotte, D. L. (1986). Implications of a two-component marble-cake mantle. *Nature* **323**, 123–127.

Ariskin, A. A., Barmina, G. S. & Frenkel, M. Ya. (1987). Simulating low-pressure tholeiite-magma crystallisation at a fixed oxygen fugacity. *Geochemistry International* **24**(5), 92–100.

Bai, Q. & Kohlstedt, D. L. (1992). Substantial hydrogen solubility in olivine and implications for water storage in the mantle. *Nature* **131**, 301–320.

Baker, M. B., Hirschmann, M. M., Ghiorso, M. S. & Stolper, E. M. (1995). Compositions of near-solidus peridotite melts from experiments and thermodynamic calculations. *Nature* **375**, 308–311.

Batiza, R. & Niu, Y. (1992). Petrology and chamber processes at the East Pacific Rise ~9°30′N. *Journal of Geophysical Research* **97**, 6779–6797.

Batiza, R. & Vanko, D. (1984). Petrology of young Pacific seamounts. *Journal of Geophysical Research* **89**, 11235–11260.

Batiza, R., Niu, Y. & Zayac, W. C. (1990). Chemistry of seamounts near the East Pacific Rise: implications for the geometry of subaxial mantle flow. *Geology* **18**, 1122–1125.

Batiza, R., Niu, Y., Karsten, J. L., Boger, W., Potts, E., Norby, L. & Butler, R. (1996). Steady and non-steady state magma chambers below the East Pacific Rise. *Geophysical Research Letters* **23**, 221–224.

Bell, D. R. (1996). Is there a global H-cycle? Evidence from H_2O and trace element systematics of Earth reservoirs. *EOS Transactions, American Geophysical Union* **77**, F806.

Bell, D. R. & Rossman, G. R. (1992). Water in Earth's mantle: the role of nominally anhydrous minerals. *Science* **255**, 1391–1397.

Blundy, J. D. (1997). Experimental study of a Kiglapait marginal rock and implications for trace element partitioning in layered intrusions. *Chemical Geology* **141**, 73–92.

Blundy, J. D., Wood, B. J. & Davies, A. (1996). Thermodynamics of rare earth element partitioning between clinopyroxene and melt in the system CaO–MgO–Al_2O_3–SiO_2. *Geochimica et Cosmochimica Acta* **60**, 359–364.

Byers, C. D., Muenow, D. W. & Garcia, M. O. (1983). Volatiles in basalts and andesites from the Galapagos spreading center, 85 to 86W. *Geochimica et Cosmochimica Acta* **47**, 1551–1558.

Castillo, P. R., Klein, E. M., Shirey, S., Bender, J., Langmuir, C. H., Batiza, R. & White, W. (2000). Petrology and Sr, Nd and Pb isotope geochemistry of MORB glasses from the 11°45′N to 15°00′N segment of the EPR. *Journal of Geophysical Research* (in press).

Danyushevsky, L. V. (2000). The effect of small amounts of H_2O on crystallisation of mid-ocean ridge and backarc basin magmas. *Journal of Volcanology and Geothermal Research* (in press).

Danyushevsky, L. V., Falloon, T. J., Sobolev, A. V., Crawford, A. J., Carroll, M. & Price, R. C. (1993). The H_2O content of basalt glasses from southwest Pacific backarc basins. *Earth and Planetary Science Letters* **117**, 347–362.

Danyushevsky, L. V., Green, D. H., Falloon, T. J. & Sobolev, A.V. (1994). The compositions of anhydrous and H_2O-undersaturated melts in equilibrium with refractory peridotites at 15 and 20 kb: implications for high-Ca boninite petrogenesis. *Mineralogical Magazine* **58A**, 209–210.

Danyushevsky, L. V., Sobolev, A. V. & Dmitriev, L. V. (1996). Estimation of the pressure of crystallisation and H_2O content of MORB and BABB glasses: calibration of an empirical technique. *Mineralogy and Petrology* **57**, 185–204.

Dixon, J. E. & Stolper, E. M. (1995) An experimental study of water and carbon dioxide solubilities in mid-ocean ridge basaltic liquids. Part II. Applications to degassing. *Journal of Petrology* **36**, 1633–1646.

Dixon, J. E., Stolper, E. M. & Holloway, J. R. (1995). An experimental study of water and carbon dioxide solubilities in mid-ocean ridge basaltic liquids. Part I. Calibration and solubility models. *Journal of Petrology* **36**, 1607–1631.

Dixon, J. E., Stolper, E. & Delaney, J. R. (1988) Infrared spectroscopic measurements of CO_2 and H_2O in Juan de Fuca Ridge basaltic glasses. *Earth and Planetary Science Letters* **90**, 87–104.

Dmitriev, L. V., Magakian, R., Danyushevsky, L. V. & Kamenetsky, V. S. (1991). New data on primitive tholeiites from the Atlantic Ocean (12th cruise of the R/V 'Academic Boris Petrov'). *Volcanology and Seismology (Vulkanologia i Seismologia)* **6**, 78–94 (in Russian).

Eggins, S. M., Kinsley, L. P. J. & Shelley, J. M. G. (1998*a*). Deposition and element fractionation processes during atmospheric pressure laser sampling for analysis by ICPMS. *Applied Surface Science* **127–129**, 278–286.

Eggins, S. M., Rudnick, R. L. & McDonough, W. F. (1998*b*). The composition of peridotites and their minerals: a laser-ablation ICP-MS study. *Earth and Planetary Science Letters* **154**, 53–71.

Falloon, T. J. & Danyushevsky, L. V. (2000). Melting of refractory mantle at 1·5, 2 and 2·5 GPa under anhydrous and H_2O-undersaturated conditions: implications for the petrogenesis of high-Ca boninites and the influence of subduction components on mantle melting. *Journal of Petrology* **41**, 257–283.

Falloon, T. J., Green, D. H., O'Neill, H. St C. & Hibberson, W. O. (1997). Experimental tests of low degree peridotite partial melt compositions: implications for the nature of anhydrous near-solidus peridotite melts at 1 GPa. *Earth and Planetary Science Letters* **152**, 149–162.

Falloon, T. J., Green, D. H., Danyushevsky, L. V. & Faul, U. H. (1999). Peridotite melting at 1·0 and 1·5 GPa: an experimental evaluation of techniques using diamond aggregates and mineral mixes for determination of near-solidus melts. *Journal of Petrology* **40**, 1343–1375.

Falloon, T. J., Danyushevsky, L. V. & Green, D. H. (2000). Peridotite melting at 1 GPa: reversal experiments on partial melt compositions produced by peridotite–basalt sandwich experiments. *Journal of Petrology* (submitted).

Ford, C. E., Russell, D. G., Groven, J. A. & Fisk, M. R. (1983). Distribution coefficients of Mg^{2+}, Fe^{2+}, Ca^{2+} and Mn^{2+} between olivine and melt. *Journal of Petrology* **24**, 256–265.

Fornari, D. J., Perfit, M. R., Allan, J. F., Batiza, R., Haymon, R., Barone, A., Smith, W. B. F., Simkin, T. & Luckman, M. (1988). Geochemical and structural studies of the Lamont seamounts: seamounts as indicators of mantle processes. *Earth and Planetary Science Letters* **89**, 63–83.

Green, D. H. (1976). Experimental testing of 'equilibrium' partial melting of peridotite under water-saturated, high-pressure conditions. *Canadian Mineralogist* **14**, 255–268.

Green, D. H. & Falloon, T. J. (1998) Pyrolite: a Ringwood concept and its current expression. In: Jackson, I. (ed.) *The Earth's Mantle: Composition, Structure, and Evolution*. Cambridge: Cambridge University Press, pp. 311–378.

Green, D. H., Falloon, T. J. & Taylor, W. R. (1987). Mantle-derived magmas—roles of variable source peridotite and variable C–H–O fluid composition. *Geochemical Society Special Publication* **1**, 139–154.

Harpp, K. S., White, W. M., Batiza, R. & Castillo, P (1991). Isotopic constraints on the East Pacific Rise magma chamber at 9°30′N. *EOS Transactions, American Geophysical Union* **72**, F496.

Hirschmann, M. M. & Stolper, E. M. (1996). A possible role for garnet pyroxenite in the origin of the 'garnet signature' in MORB. *Contributions to Mineralogy and Petrology* **124**, 185–208.

Hirth, G. & Kohlstedt, D. (1996). Water in the oceanic upper mantle: implications for rheology, melt extraction and the evolution of the lithosphere. *Earth and Planetary Science Letters* **144**, 93–108.

Hofmann, A. W. (1988) Chemical differentiation of the Earth: the relationship between mantle, continental crust, and oceanic crust. *Earth and Planetary Science Letters* **90**, 297–314.

Jambon, A. & Zimmermann, J. L. (1990). Water in oceanic basalts: evidence for dehydration of recycled crust. *Earth and Planetary Science Letters* **101**, 323–331.

Jarosewich, E. J., Nelen, J. A. & Norberg, J. A. (1980). Reference samples for electron microprobe analyses. *Geostandards Newsletter* **4**, 257–258.

Johnson, K. T. M., Dick, H. J. B. & Shimizu, N. (1990). Melting in the oceanic upper mantle: an ion microprobe study of diopside in abyssal peridotites. *Journal of Geophysical Research* **95**, 2661–2678.

Kinzler, R. J. (1997). Melting of mantle peridotite at pressures approaching the spinel to garnet transition: application to mid-ocean ridge basalt petrogenesis. *Journal of Geophysical Research* **102**, 853–874.

Kinzler, R. J. & Grove, T.L. (1992). Primary magmas of mid-ocean ridge basalts 1. Experiments and methods. *Journal of Geophysical Research* **97**, 6907–6926.

Klein, E. M. & Langmuir, C. H. (1987). Global correlations of ocean ridge basalt chemistry with axial depth and crustal thickness. *Journal of Geophysical Research* **92**, 8089–8115.

Kohn, S. C. (1996). Solubility of H_2O in nominally anhydrous mantle minerals using ^1H MAS NHR. *American Mineralogist* **81**, 1523–1526.

Langmuir, C. H., Bender, J. F. & Batiza, R. (1986). Petrological and tectonic segmentation of the East Pacific Rise, 5°30′–14°30′N. *Nature* **322**, 422–429.

Langmuir, C. H., Klein, E. M. & Plank, T. (1992). Petrological systematics of mid-ocean ridge basalts: constraints on melt generation beneath ocean ridges. In: Phipps Morgan, J., Blackman, D. K. & Sinton, J. M. (eds) *Mantle Flow and Melt Generation at Mid-ocean Ridges. Geophysical Monograph, American Geophysical Union* **71**, 183–280.

Longerich, H. P., Jackson, S. E. & Gunther, D. (1996). Laser ablation inductively coupled plasma mass spectrometric transient signal data acquisition and analyte concentration calculation. *Journal of Analytical and Atomic Spectroscopy* **11**, 899–904.

Lundstrom, C. C., Sampson, D. E., Perfit, M. R., Gill, J. & Williams, Q. (1999). Insights into mid-ocean ridge basalt petrogenesis: U-series disequilibria from the Siqueiros Transform, Lamont Seamounts, and East Pacific Rise. *Journal of Geophysical Research* **104**, 13035–13048.

Mahoney, J. J., Sinton, J. M., Kutz, M. D., Macdougall, J. D., Spencer, K. J. & Lugmair, G. W. (1994). Isotope and trace element characteristics of a super-fast spreading ridge: East Pacific rise, 13–23°S. *Earth and Planetary Science Letters* **121**, 173–193.

McKay, G., Le, L., Wagstaff, J. & Crozaz, G. (1994). Experimental partitioning of rare earth elements and strontium: constraints on petrogenesis and redox conditions during crystallisation of Antarctic angrite Lewis Cliff 86010. *Geochimica et Cosmochimica Acta* **58**, 2911–2919.

McNeill, A. W. & Danyushevsky, L. V. (1996). Compositions and crystallisation temperatures of primary melts for hole 896A, Leg 148, basalts: evidence from melt inclusion studies. In: Alt, J. C., Kinoshita, H., Stokking, L. B. & Michael, P. J. (eds) *Proceedings of the Ocean Drilling Program, Scientific Reports 148*. College Station, TX: Ocean Drilling Program, pp. 21–35.

Michael, P. J. (1988). The concentration, behaviour and storage of H_2O in the suboceanic upper mantle: implications for mantle metasomatism. *Geochimica et Cosmochimica Acta* **52**, 555–566.

Michael, P. J. (1995). Regionally distinctive sources of depleted MORB: evidence from trace elements and H_2O. *Earth and Planetary Science Letters* **131**, 301–320.

Michael, P. J. & Chase, R. L. (1987). The influence of primary magma composition, H_2O and pressure on mid-ocean ridge basalt differentiation. *Contributions to Mineralogy and Petrology* **96**, 245–263.

Michael, P. J. & Schilling, J.-G. (1989). Chlorine in mid-ocean ridge magmas: evidence for assimilation of seawater-influenced components. *Geochimica et Cosmochimica Acta* **53**, 3131–3143.

Natland, J. H. (1989). Partial melting of a lithologically heterogeneous mantle: inferences from crystallisation histories of magnesian abyssal tholeiites from the Siqueiros Fracture Zone. In: Saunders, A. D. & Norry, M. J. (eds) *Magmatism in the Ocean Basins. Geological Society, London, Special Publication* **42**, 41–70.

Niu, Y. & Batiza, R. (1991). An empirical method for calculating melt compositions produced beneath mid-ocean ridges: application for axis and off-axis (seamount) melting. *Journal of Geophysical Research* **96**, 21753–21777.

Niu, Y. & Batiza, R. (1997). Trace element evidence from seamounts for recycled ocean crust in the Eastern Pacific mantle. *Earth and Planetary Science Letters* **148**, 471–484.

Niu, Y., Waggoner, D. G., Sinton, J. M. & Mahoney, J. J. (1996). Mantle source heterogeneity and melting processes beneath seafloor spreading centers: the East Pacific Rise, 18°–19°S. *Journal of Geophysical Research* **101**, 27711–27733.

Niu, Y., Collerson, K. D., Batiza, R., Wendt, J. I. & Regelous, M. (1999). Origin of enriched-type mid-ocean ridge basalt at ridges far from mantle plumes: the East Pacific Rise at 11°20′N. *Journal of Geophysical Research* **104**, 7067–7087.

Palmer, J., Sempere, J.-C., Christie, D. M. & Phipps-Morgan, J. (1993). Morphology and technotics of the Australian–Antarctic Discordance between 123°E and 128°E. *Marine Geophysical Research* **15**, 121–151.

Papike, J. J., Fowler, G. W., Shearer, C. K. & Layne, G. D. (1996). Ion microprobe investigation of plagioclase and orthopyroxene from lunar Mg-suite norites: implications for calculating parental melt REE concentrations and for assessing postcrystallization REE redistribution. *Geochimica et Cosmochimica Acta* **60**, 3967–3978.

Perfit, M. R., Fornari, D. J., Smith, M. C., Bender, J. F., Langmuir, C. H. & Haymon, R. M. (1994). Small-scale spatial and temporal variations in mid-ocean ridge crest magmatic processes. *Geology* **22**, 375–379.

Phinney, W. C. & Morrison, D. A. (1990). Partition coefficients for calcic plagioclase: implications for Archean anorthosites. *Geochimica et Cosmochimica Acta* **54**, 1639–1654.

Prinzhofer, A., Lewin, E. & Allègre, C. J. (1989). Stochastic melting of the marble cake mantle: evidence from local study of the East Pacific Rise at 12°50′N. *Earth and Planetary Science Letters* **92**, 189–206.

Pyle, D.G. (1994). Geochemistry of mid-ocean ridge basalt within and surrounding the Australia–Antarctic Discordance. Ph.D. Dissertation, Oregon State University, Corvallis, 178 pp.

Pyle, D. G., Christie, D. M. & Mahoney, J. J. (1992). Resolving an isotopic boundary within the Australian–Antarctic Discordance. *Earth and Planetary Science Letters* **112**, 161–178.

Regelous, M., Niu, Y., Wendt, J. I., Batiza, R., Grieg, A. & Collerson, K. D. (1999). Variations in the geochemistry of magmatism on the East Pacific Rise at 10°30′N since 800 ka. *Earth and Planetary Science Letters* **168**, 45–63.

Reynolds, J. R. & Langmuir, C. H. (1997). Petrological systematics of the Mid-Atlantic Ridge south of Kane: implications for ocean crust formation. *Journal of Geophysical Research* **102**, 14915–14946.

Robinson, J. A. C., Wood, B. J. & Blundy, J. D. (1998). The beginning of melting of fertile and depleted peridotite at 1·5 GPa. *Earth and Planetary Science Letters* **155**, 97–111.

Saunders, A. D., Norry, M. J. & Tarney, J. (1988). Origin of MORB and chemically-depleted mantle reservoirs: trace element constraints. *Journal of Petrology, Special Lithosphere Issue* 415–445.

Schmidt, M. W. & Poli, S. (1998). Experimentally based water budgets for dehydrating slabs and consequences for arc magma generation. *Earth and Planetary Science Letters* **163**, 361–379.

Sims, K. W. W. & DePaolo, D. J. (1997). Inferences about mantle magma sources from incompatible element concentration ratios in oceanic basalts. *Geochimica et Cosmochimica Acta* **61**, 765–784.

Sinton, J. M. & Fryer, P. (1987). Mariana Trough lavas from 18°N: implications for the origin of back-arc basalts. *Journal of Geophysical Research* **92**, 12782–12802.

Sobolev, A. V. & Chaussidon, M. (1996). H_2O concentrations in primary melts from supra-subduction zones and mid-ocean ridges: implications for H_2O storage and recycling in the mantle. *Earth and Planetary Science Letters* **137**, 45–55.

Sobolev, A. V. & Shimizu, N. (1993). Ultra-depleted primary melt included in an olivine from the Mid-Atlantic Ridge. *Nature* **363**, 151–154.

Sobolev, A. V., Danyushevsky, L. V., Dmitriev, L. V. & Suschevskaya, N. M. (1989). High-alumina magnesian tholeiite as the primary basalt magma at mid-ocean ridge. *Geochemistry International* **26**(5), 128–133.

Sun, S.-S. & McDonough, W. F. (1989). Chemical and isotopic systematics of oceanic basalts: implications for mantle composition and processes. In: Saunders, A. D. & Norry, M. J. (eds) *Magmatism in the Ocean Basins. Geological Society, London, Special Publication* **42**, 313–345.

Weaver, J. S. & Langmuir, C. H. (1990). Calculation of phase equilibrium in mineral–melt systems. *Computers and Geosciences* **16**, 1–19.

Wood, B. J. & Blundy, J. D. (1997). A predictive model for rare earth element partitioning between clinopyroxene and anhydrous silicate melt. *Contributions to Mineralogy and Petrology* **129**, 166–181.

Zindler, A., Staudigel, H. & Batiza, R. (1984). Isotope and trace element geochemistry of young Pacific seamounts: implications for the scale of mantle heterogeneity. *Earth and Planetary Science Letters* **70**, 175–195.

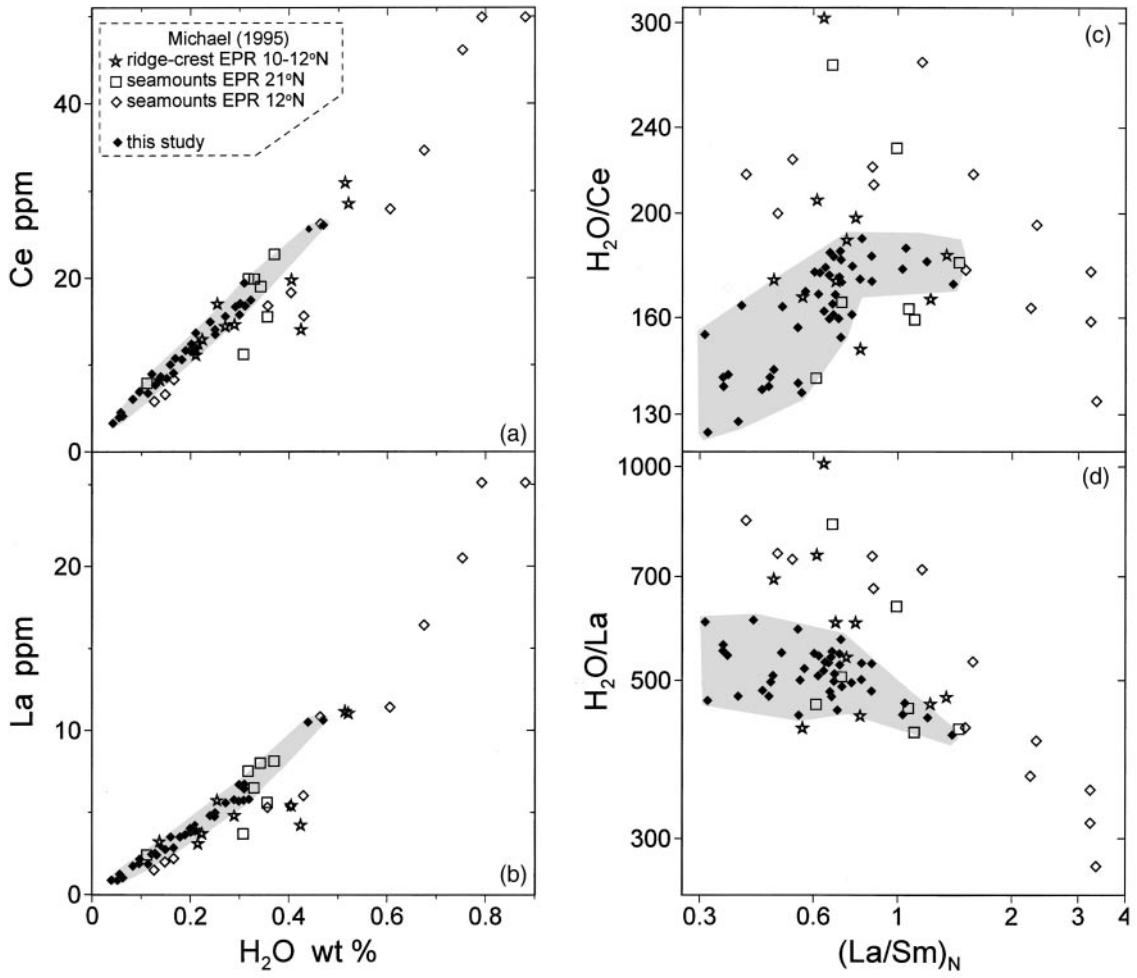

Fig. A1. Comparison of our results for 9–11°N EPR glasses with previously published data from surrounding areas (Michael, 1995). In (c) and (d), normalization to primitive mantle of Sun & McDonough (1989).

APPENDIX A: COMPARISON OF OUR RESULTS FOR GLASSES FROM THE EPR WITH PREVIOUSLY PUBLISHED H_2O CONTENTS OF GLASSES FROM SURROUNDING AREAS

The H_2O contents of MORB glasses from the EPR close to the area of this study were previously reported by several workers and were compiled by Michael (1995). These data are compared with the results of our study in Fig. A1.

In general, the data from Michael (1995) define a single covariation trend between H_2O and the LREE (Fig. A1a and b), which overlaps with our data. However, the scatter in the literature data is significantly larger. There are several possible reasons for this: (1) H_2O in the ridge-crest glasses from Michael (1995) was measured by FTIR spectroscopy, whereas trace elements were analysed on whole-rock samples and no correction has been introduced to account for possible difference between glass and whole-rock compositions in these samples (Michael, 1995); (2) H_2O in the seamount glasses was determined by Aggrey *et al.* (1988) by high-temperature mass spectroscopy, whereas trace-element data represent a mixture of glass and whole-rock analyses, and again, no correction for possible differences in compositions has been used. Although we demonstrate in this paper that systematic regional differences in relative H_2O contents exist in the global mid-ocean ridge system on a similar scale to that displayed by the EPR data of Michael (1995), we believe that the scatter in the literature data

Table B1: Distribution coefficients used in this study

Element	Plagioclase An_{90}	Plagioclase An_{70}	Clinopyroxene *mg*-no. = 80, Al_2O_3 ~ 3–4 wt %
H_2O	0	0	0
K_2O	0·13	0·13	0·005
La	0·05	0·13	0·07
Ce	0·04	0·1	0·12
Sm	0·02	0·05	0·43

References: Phinney & Morrison (1990); McKay *et al.* (1994); Papike *et al.* (1996); Blundy (1997).

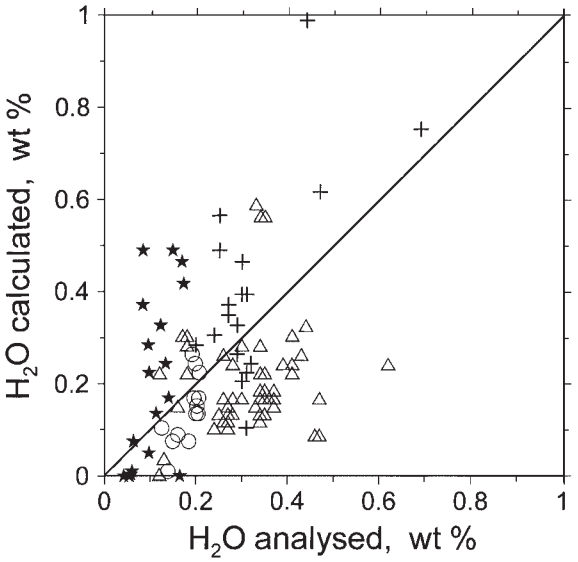

Fig. B1. Comparison of analysed H_2O contents in the studied glasses with calculated H_2O contents using the technique of Danyushevsky *et al.* (1996). Symbols as in Fig. 1. (See text for discussion.)

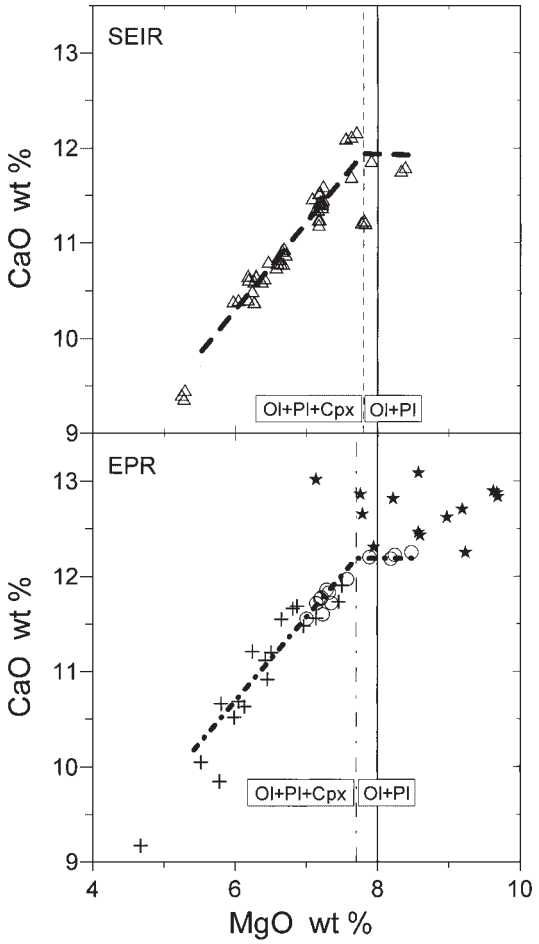

Fig. B2. CaO vs MgO for the studied glasses. Symbols as in Fig. 1. Bold dash–dot line and the bold dashed line show the bend in the fractionation path reflecting the incoming of clinopyroxene for the EPR and SEIR glasses, respectively. Thin vertical lines are the MgO contents at which this change occurs (7·7 for the EPR glasses and 7·8 for the SEIR glasses). Continuous line at 8 wt % MgO is the target for the recalculation procedure. It should be noted that the Lamont Seamount glasses have not reached clinopyroxene saturation. (See text for discussion.)

is analytical. Overall higher H_2O at a given LREE content for the data of Michael (1995) (Fig. A1a and b) may reflect differences between H_2O measuring techniques, or alternatively systematically lower LREE at a given H_2O content may reflect presence of microlites in the analysed samples. Probably both factors contributed to the observed differences, as H_2O/K_2O values (not shown on Fig. 1A) overlap with our data.

APPENDIX B: CORRECTIONS FOR FRACTIONATION

Glass compositions from Table 1 and from high-*P* experimental studies (Falloon *et al.*, 1997, 1999, 2000; Robinson *et al.*, 1998) were recalculated to 8 wt % MgO assuming fractional crystallization and using the computer package PETROLOG with the model of Danyushevsky (2000). If a glass has <8 wt % MgO, its composition is recalculated to 8 wt % MgO by modelling the reverse of fractional crystallization. The model of Danyushevsky (2000) uses the olivine–melt equilibrium model of Ford *et al.* (1983) and modified plagioclase–melt and clinopyroxene–melt models of Weaver & Langmuir (1990) and Ariskin *et al.* (1987), respectively. Modifications involve corrections to calculated T of plagioclase and clinopyroxene crystallization, and have been described by Danyushevsky *et al.* (1996) and Danyushevsky (2000). The model accounts for the effect of H_2O in suppressing plagioclase crystallization, and for the effect of P in enhancing

clinopyroxene crystallization. The model of Danyushevsky (2000) calculates Si, Mg, Fe, Mn, Ca, and Cr contents in liquidus olivine; Si, Al, Ca, Na, Mg, and Fe contents in plagioclase; Si, Ti, Al, Mg, Fe, Ca, Na, Mn, and Cr in clinopyroxene. Incompatible trace-element K_d values for plagioclase and clinopyroxene used in calculations are shown in Table B1. K_d values for olivine were assumed to be zero for all incompatible elements.

All calculations were performed assuming that natural glass compositions reflect liquids that evolved along either an olivine + plagioclase cotectic, or an olivine + plagioclase + clinopyroxene cotectic. The technique of Danyushevsky *et al.* (1996) [refined by Danyushevsky (2000)] allows an estimation of the H_2O content in a MORB melt if this melt is saturated in both olivine and plagioclase. This is achieved by calculating the difference between the 1 atm anhydrous liquidus temperatures of plagioclase and olivine and then recalculating it to the H_2O contents using the calibration provided by Danyushevsky (2000). Figure B1 shows a reasonable agreement between analysed H_2O contents in the studied glasses and H_2O contents predicted by the model of Danyushevsky (2000) assuming that these glasses are olivine–plagioclase cotectic. The accuracy of the model of Danyushevsky (2000) in predicting the fractionation path of MORB magmas is evaluated by comparing the calculated paths with the trends observed in natural glass suites that have evolved by fractionation only. PETROLOG is available from the first author.

Melt MgO contents at the moment when clinopyroxene appears on the liquidus were estimated for each suite using the bend of the MgO–CaO trend. For the normal crust samples from the EPR, melt MgO content was estimated to be 7·8 wt %; for the SEIR samples, 7·7 wt % (Fig. B2). For glasses corresponding to the olivine + plagioclase + clinopyroxene cotectic, crystallization P was estimated using the model of Danyushevsky *et al.* (1996). For glasses along the olivine + plagioclase cotectic, calculations were performed at 10 MPa. The same P was used for recalculating high-P experimental melts to 8 wt % MgO.